

Electroweak Contributions to Squark Pair Production at the LHC

SASCHA BORNHAUSER^{1,2}, MANUEL DREES^{1,2}, HERBI K. DREINER¹ and JONG SOO KIM¹

¹*Physikalisches Institut, Universität Bonn, Nussallee 12, D53115 Bonn, Germany*

²*KIAS, School of Physics, Seoul 130-012, Korea*

Abstract

In this paper we compute electroweak contributions to the production of squark pairs at hadron colliders. These include the exchange of electroweak gauge bosons in the s -channel as well as electroweak gaugino exchange in the t - and/or u -channel. In many cases these can interfere with the dominant QCD contributions. As a result, we find sizable contributions to the production of two $SU(2)$ doublet squarks. At the LHC, they amount to 10 to 20% for typical mSUGRA (or CMSSM) scenarios, but in more general scenarios they can vary between -40 and $+55\%$, depending on size and sign of the $SU(2)$ gaugino mass. The electroweak contribution to the total squark pair production rate at the LHC is about 3.5 times smaller.

1 Introduction

The Standard Model (SM) of particle physics, while very successful, suffers from several theoretical as well as phenomenological problems. Many of these can be solved by postulating the existence of superpartners [1] to all known elementary particles, with masses at or below the TeV scale. This solves the (technical part of the) hierarchy problem by stabilizing scalar masses – in particular, the mass of the SM Higgs boson – against quadratically divergent quantum corrections [2]. Superstring theory, which is our currently most promising avenue towards a perturbative theory of quantum gravity, also requires supersymmetry (albeit not necessarily at the TeV scale).

The simplest possibly realistic supersymmetric model is known as the Minimal Supersymmetric extension of the Standard Model (MSSM). In addition to the virtues described above, it also allows for one-step unification of the three gauge couplings of the SM [3]. Moreover, it has several phenomenological advantages. It can naturally accommodate [4] the existence of Dark Matter, which probably accounts for $\sim 80\%$ of all matter in the Universe [5]. It easily provides [6] the additional quantum correction to the anomalous magnetic moment of the muon that seems to be required by current data [7], if the SM prediction [8] based on $e^+e^- \rightarrow \text{hadrons}$ data can be trusted. Finally, recent fits to precision electroweak data indicate a slight preference of the MSSM over the SM [9].

The idea that superparticles exist near the TeV scale will be tested decisively at the LHC [10]. Here the production of squark pairs is expected to play an important role. This final state can be accessed via leading order strong interactions, i.e. the cross section is $\mathcal{O}(\alpha_s^2)$. Moreover, there are contributions with two valence quarks in the initial state. Since valence quarks have the hardest of all parton distribution functions (pdf's), i.e. show the slowest fall-off as Bjorken- $x \rightarrow 1$, very massive quark pairs can be produced with appreciable rate. For example, the leading order (LO) QCD cross section for the production of degenerate first and second generation squarks with mass 1 TeV still exceeds 0.5 pb, leading to 5,000 events per year even at low luminosity. One can thus expect that the total cross section for squark pair production will eventually be measured with a statistical uncertainty of a few percent. Accurate predictions for this quantity are therefore obviously of great interest.

The leading order QCD cross section for squark pair production at hadron colliders has first been calculated in the 1980s [11]. The NLO QCD corrections were calculated about ten years ago [12]. The remaining uncertainty from yet higher order QCD corrections should be at the ten percent level.

In this paper we compute the complete leading order electroweak contributions to squark pair production at hadron colliders. Since in many cases interference with QCD amplitudes is possible, this yields contributions of $\mathcal{O}(\alpha_S\alpha_W)$ as well as of $\mathcal{O}(\alpha_W^2)$, where α_W is a weak gauge coupling. We find that these change the total cross section by only a few percent if at least one of the produced squarks is an $SU(2)$ singlet. On the other hand, the cross section for the production of two $SU(2)$ doublet squarks is changed by 10 to 20% in typical mSUGRA [13] (or CMSSM) scenarios [14]; in scenarios without gaugino mass unification [15] the corrections can exceed 50%.¹ These new contributions peak at small transverse momentum of the produced

¹Electroweak contributions to squark production have recently also been computed in ref.[16]. However, the emphasis of that paper is on flavor observables; the impact on the total cross section, which is our main focus, is not discussed there. Ref.[17] also computes electroweak contributions to squark pair production. However,

squark; they can therefore not be subsumed in a constant “ k –factor”.

The remainder of this article is organized as follows. In the following Section we give explicit expressions for the squared amplitudes for all processes with two quarks in the initial state and two squarks in the final state, where anti–particles are included. In Sec. 3 we present numerical results for the total cross section as well as the $p_{T,\tilde{q}}$ distribution, before concluding in Sec. 4. A list of employed couplings is given in the Appendix.

2 Formalism

In this section we present analytical results for the leading–order parton–level squared matrix elements for the production of two (anti–)squarks from two (anti–)quarks in the initial state. We will first give a ‘master formula’ in terms of general s –, t – and u –channel diagrams. We then describe the different processes by listing the contributing types of diagrams, and specifying the couplings in terms of elementary vertex factors. The latter are listed in an Appendix.

2.1 General Formula

In this subsection we present the squared spin and color averaged matrix elements for squark pair production. We do not consider gluon fusion. Since we only consider production of first and second generation squarks, we ignore all quark mass effects, including mixing between $SU(2)$ doublet and singlet squarks.

We begin by specifying functions that describe the contributions from various kinds of matrix elements. Φ and χ describe squared t – and u –channel (gaugino exchange) diagrams², while Ψ describes the interference between a t – channel and a u –channel diagram. Similarly, s –channel (gauge boson exchange) and the interference between s – and t –channel diagrams are described by Υ and Ω , respectively:

$$\begin{aligned}\Phi(\tilde{q}_{i\alpha}, \tilde{q}'_{j\beta}, a) &= \frac{1}{4} \sum_{l,k} c_a(l, k) \frac{1}{\hat{t} - m_l^2} \frac{1}{\hat{t} - m_k^2} \left\{ A(l, k, \tilde{q}_{i\alpha}, \tilde{q}'_{j\beta}) \right. \\ &\quad \left. \times (\hat{t}\hat{u} - m_{\tilde{q}_{i\alpha}}^2 m_{\tilde{q}'_{j\beta}}^2) + B(l, k, \tilde{q}_{i\alpha}, \tilde{q}'_{j\beta}) m_l m_k \hat{s} \right\}, \\ \chi(\tilde{q}_{i\alpha}, \tilde{q}'_{j\beta}, a) &= \frac{1}{4} \sum_{l,k} c_a(l, k) \frac{1}{\hat{u} - M_l^2} \frac{1}{\hat{u} - M_k^2} \left\{ C(l, k, \tilde{q}_{i\alpha}, \tilde{q}'_{j\beta}) \right. \\ &\quad \left. \times (\hat{t}\hat{u} - m_{\tilde{q}_{i\alpha}}^2 m_{\tilde{q}'_{j\beta}}^2) + D(l, k, \tilde{q}_{i\alpha}, \tilde{q}'_{j\beta}) M_l M_k \hat{s} \right\}, \\ \Psi(\tilde{q}_{i\alpha}, \tilde{q}'_{j\beta}, a) &= \frac{1}{4} \sum_{l,k} c_a(l, k) \frac{1}{\hat{t} - m_l^2} \frac{1}{\hat{u} - M_k^2} F(l, k, \tilde{q}_{i\alpha}, \tilde{q}'_{j\beta}) m_l M_k \hat{s},\end{aligned}$$

their emphasis is on tests of CP violation; besides, the analytical results in that paper seem to contain several errors (e.g., non–vanishing interference between gluon and photon exchange in the s –channel).

²This includes products of two different t – or u –channel diagrams.

$$\begin{aligned}
\Upsilon(q_g, q'_h, \tilde{q}_{i\alpha}, \tilde{q}'_{j\beta}, a) &= \frac{1}{4} \sum_{l,k} c_a(l, k) \frac{1}{\hat{s} - M_l^2} \frac{1}{\hat{s} - M_k^2} G(l, k, q_g, q'_h, \tilde{q}_{i\alpha}, \tilde{q}'_{j\beta}) \\
&\quad \times \left\{ (m_{\tilde{q}'_{j\beta}}^2 - m_{\tilde{q}_{i\alpha}}^2 + \hat{t} - \hat{u})(m_{\tilde{q}'_{j\beta}}^2 - m_{\tilde{q}_{i\alpha}}^2 + \hat{u} - \hat{t}) \right. \\
&\quad \left. - \hat{s}(2m_{\tilde{q}_{i\alpha}}^2 + 2m_{\tilde{q}'_{j\beta}}^2 - \hat{s}) \right\}, \\
\Omega(q_g, q'_h, \tilde{q}_{i\alpha}, \tilde{q}'_{j\beta}, a) &= -\frac{1}{4} \sum_{l,k} c_a(l, k) \frac{1}{\hat{s} - M_l^2} \frac{1}{\hat{t} - m_k^2} H(l, k, q_g, q'_h, \tilde{q}_{i\alpha}, \tilde{q}'_{j\beta}) \\
&\quad \times \left\{ (m_{\tilde{q}'_{j\beta}}^2 - \hat{t})(m_{\tilde{q}_{i\alpha}}^2 - m_{\tilde{q}'_{j\beta}}^2 + \hat{u} - \hat{t}) \right. \\
&\quad \left. - \hat{s}(\hat{s} - 3m_{\tilde{q}'_{j\beta}}^2 - m_{\tilde{q}_{i\alpha}}^2) + (m_{\tilde{q}'_{j\beta}}^2 - \hat{u})(m_{\tilde{q}_{i\alpha}}^2 - m_{\tilde{q}'_{j\beta}}^2 + \hat{t} - \hat{u}) \right\}. \tag{1}
\end{aligned}$$

\hat{t} , \hat{u} and \hat{s} denote the partonic Mandelstam variables. $m_{l,k}$, $M_{l,k}$ and $m_{\tilde{q}_{i\alpha}, j\beta}$ are the masses of the propagating particles and the final states squarks, respectively; we use capital letters for the masses of particles exchanged in the u - or s -channel, and lower case letters for masses in t -channel propagators. The electrically neutral gauge bosons, all of which can contribute to the same processes, are labeled through the indices $l, k = 1, 2, 3$ for γ , Z and gluon, respectively; W -boson exchange can only occur in different reactions than the exchange of the neutral gauge bosons. Similarly, the four neutralinos and the gluino, which can contribute to the same process, are labeled by $l, k = 1, 2, 3, 4, 5$; alternatively, the two charginos are represented by $l, k = 1, 2$. The flavour of the quarks and squarks is given by $q, q' = u, d$. $g, h, i, j = 1, 2$ are generation indices. $\alpha, \beta = 1, 2$ label $SU(2)$ doublet (L -type) and singlet (R -type) squarks, respectively. $c_a(l, k)$ are the colour factors for the different contributions, where a labels the various exchange topologies; note that unlike l and k , a is not summed. Finally, the functions A, B, C, D, F, G and H are products of the various coupling constants appearing in the matrix elements for the different processes. Their general structure is given by

$$\begin{aligned}
A(l, k, \tilde{q}_{i\alpha}, \tilde{q}'_{j\beta}) &= a(l, \tilde{q}_{i\alpha})a(k, \tilde{q}_{i\alpha})b'(l, \tilde{q}'_{j\beta})b'(k, \tilde{q}'_{j\beta}) \\
&\quad + b(l, \tilde{q}_{i\alpha})b(k, \tilde{q}_{i\alpha})a'(l, \tilde{q}'_{j\beta})a'(k, \tilde{q}'_{j\beta}), \\
B(l, k, \tilde{q}_{i\alpha}, \tilde{q}'_{j\beta}) &= a(l, \tilde{q}_{i\alpha})a(k, \tilde{q}_{i\alpha})a'(l, \tilde{q}'_{j\beta})a'(k, \tilde{q}'_{j\beta}) \\
&\quad + b(l, \tilde{q}_{i\alpha})b(k, \tilde{q}_{i\alpha})b'(l, \tilde{q}'_{j\beta})b'(k, \tilde{q}'_{j\beta}), \\
C(l, k, \tilde{q}_{i\alpha}, \tilde{q}'_{j\beta}) &= c(l, \tilde{q}_{j\beta})c(k, \tilde{q}_{j\beta})d'(l, \tilde{q}'_{i\alpha})d'(k, \tilde{q}'_{i\alpha}) \\
&\quad + d(l, \tilde{q}_{j\beta})d(k, \tilde{q}_{j\beta})c'(l, \tilde{q}'_{i\alpha})c'(k, \tilde{q}'_{i\alpha}), \\
D(l, k, \tilde{q}_{i\alpha}, \tilde{q}'_{j\beta}) &= c(l, \tilde{q}_{j\beta})c(k, \tilde{q}_{j\beta})c'(l, \tilde{q}'_{i\alpha})c'(k, \tilde{q}'_{i\alpha}) \\
&\quad + d(l, \tilde{q}_{j\beta})d(k, \tilde{q}_{j\beta})d'(l, \tilde{q}'_{i\alpha})d'(k, \tilde{q}'_{i\alpha}), \\
F(l, k, \tilde{q}_{i\alpha}, \tilde{q}'_{j\beta}) &= a(l, \tilde{q}_{i\alpha})c(k, \tilde{q}_{j\beta})a'(l, \tilde{q}'_{j\beta})c'(k, \tilde{q}'_{i\alpha}) \\
&\quad + b(l, \tilde{q}_{i\alpha})d(k, \tilde{q}_{j\beta})b'(l, \tilde{q}'_{j\beta})d'(k, \tilde{q}'_{i\alpha}), \\
G(l, k, q_g, q'_h, \tilde{q}_{i\alpha}, \tilde{q}'_{j\beta}) &= c(l, \tilde{q}_{i\alpha}, \tilde{q}'_{j\beta})c(k, \tilde{q}_{i\alpha}, \tilde{q}'_{j\beta}) \\
&\quad \times \left\{ e(l, q_g, q'_h)e(k, q_g, q'_h) + f(l, q_g, q'_h)f(k, q_g, q'_h) \right\}, \\
H(l, k, q_g, q'_h, \tilde{q}_{i\alpha}, \tilde{q}'_{j\beta}) &= c(l, \tilde{q}_{i\alpha}, \tilde{q}'_{j\beta}) \left\{ e(l, q_g, q'_h)b'(k, \tilde{q}'_{j\beta})a(k, \tilde{q}_{i\alpha}) \right. \\
&\quad \left. + f(l, q_g, q'_h)a'(k, \tilde{q}'_{j\beta})b(k, \tilde{q}_{i\alpha}) \right\}. \tag{2}
\end{aligned}$$

Here l and k again label the exchanged (s)particles. a, b, c, d, a', b', c' and d' denote couplings

of the relevant gaugino–quark–squark vertices; a, c, a' and c' denote left-handed couplings, i.e. the corresponding vertex factors are multiplied with the left-chiral projector $P_L = (1 - \gamma_5)/2$, while b, d, b' and d' denote right-handed couplings. Similarly, e and f are left- and right-handed gauge boson–quark–anti-quark couplings, respectively, and c is a gauge boson–squark–anti-squark coupling.

In the subsequent description of the contributing classes of subprocesses we will specify the contributing diagrams, color factors, and couplings; explicit expressions for the latter are given in the Appendix.

2.2 $qq' \rightarrow \tilde{q}\tilde{q}'$

We begin by discussing processes with two squarks or two anti-squarks in the final state. There are no s -channel contributions to this class of processes. We take all squark–quark–neutralino and squark–quark–gluino couplings to be flavor–diagonal. Similarly, we ignore CKM mixing for charged currents, i.e. we assume that quark–squark–chargino couplings only occur within one generation. In the given class of reactions the flavor in the initial and final state is therefore always the same.

2.2.1 $u_i u_j \rightarrow \tilde{u}_{i\alpha} \tilde{u}_{j\beta}$

These processes proceed through the exchange of a neutralino or gluino in the t - or u -channel, as shown in Fig. 1.

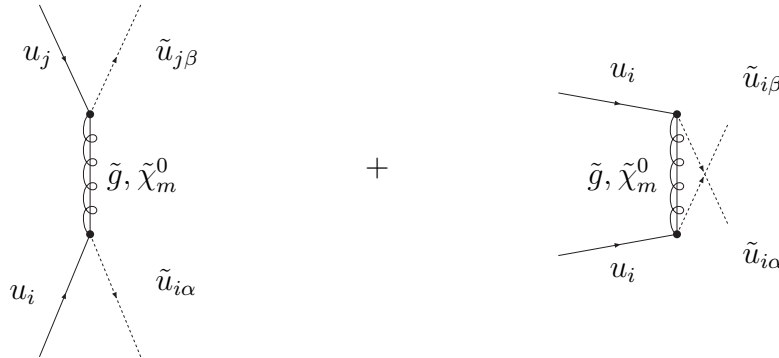


Figure 1: Feynman diagrams contributing to $u_i u_j \rightarrow \tilde{u}_{i\alpha} \tilde{u}_{j\beta}$. Here i and j are flavor indices, while α and β label the ‘chirality’ of the squarks, with 1 (2) standing for L -type (R -type) squarks. The index $m \in \{1, 2, 3, 4\}$ labels the exchanged neutralino. The second, u -channel, diagram only exists for $i = j$.

In the notation of Eq.(2) the squared spin- and color-averaged matrix element is given by

$$|\overline{M}|^2 = \Phi(\tilde{u}_{i\alpha}, \tilde{u}_{j\beta}, 1) + \chi(\tilde{u}_{i\alpha}, \tilde{u}_{i\beta}, 1)\delta_{ij} + \Psi(\tilde{u}_{i\alpha}, \tilde{u}_{i\beta}, 2)\delta_{ij}. \quad (3)$$

If the final state squarks are identical, a statistics factor of $\frac{1}{2}$ must be included. The colour factors of the t - and the u -channel are given by $c_1(l, k)$, while the factors for the interference term are given by $c_2(l, k)$. Explicitly,

$$c_1(l, k) = \begin{pmatrix} 1 & 1 & 1 & 1 & 0 \\ 1 & 1 & 1 & 1 & 0 \\ 1 & 1 & 1 & 1 & 0 \\ 1 & 1 & 1 & 1 & 0 \\ 0 & 0 & 0 & 0 & 2/9 \end{pmatrix}, \quad c_2(l, k) = \begin{pmatrix} 1 & 1 & 1 & 1 & 4/9 \\ 1 & 1 & 1 & 1 & 4/9 \\ 1 & 1 & 1 & 1 & 4/9 \\ 1 & 1 & 1 & 1 & 4/9 \\ 4/9 & 4/9 & 4/9 & 4/9 & -2/27 \end{pmatrix}. \quad (4)$$

The relevant neutralino–squark–quark and gluino–squark–quark-couplings to be inserted in Eqs.(2) are

$$\begin{aligned} a(l, \tilde{u}_{i\alpha}) &= a_{\tilde{\chi}_l^0/\tilde{g}}(\tilde{u}_{i\alpha}), & b(l, \tilde{u}_{i\alpha}) &= b_{\tilde{\chi}_l^0/\tilde{g}}(\tilde{u}_{i\alpha}), \\ a'(l, \tilde{u}_{j\beta}) &= a_{\tilde{\chi}_l^0/\tilde{g}}(\tilde{u}_{j\beta}), & b'(l, \tilde{u}_{j\beta}) &= b_{\tilde{\chi}_l^0/\tilde{g}}(\tilde{u}_{j\beta}), \\ c(l, \tilde{u}_{i\beta}) &= a_{\tilde{\chi}_l^0/\tilde{g}}(\tilde{u}_{i\beta}), & d(l, \tilde{u}_{i\beta}) &= b_{\tilde{\chi}_l^0/\tilde{g}}(\tilde{u}_{i\beta}), \\ c'(l, \tilde{u}_{i\alpha}) &= a_{\tilde{\chi}_l^0/\tilde{g}}(\tilde{u}_{i\alpha}), & d'(l, \tilde{u}_{i\alpha}) &= b_{\tilde{\chi}_l^0/\tilde{g}}(\tilde{u}_{i\alpha}). \end{aligned} \quad (5)$$

As indicated earlier, $l \in \{1, 2, 3, 4\}$ refers to the l -th neutralino, while $l = 5$ refers to the gluino. Explicit expressions for the neutralino and gluino couplings appearing in Eq.(5) can be found in the Appendix, Eqs.(30) and (31).

Eqs.(3) and (4) also hold for the charge conjugate process. However, we have to use the appropriate anti-(s)quark couplings in Eqs.(2), which are given by

$$a_{\tilde{\chi}_l^0/\tilde{g}}(\tilde{\bar{u}}_{i\alpha}) = \left[b_{\tilde{\chi}_l^0/\tilde{g}}(\tilde{u}_{i\alpha}) \right]^*, \quad b_{\tilde{\chi}_l^0/\tilde{g}}(\tilde{\bar{u}}_{i\alpha}) = \left[a_{\tilde{\chi}_l^0/\tilde{g}}(\tilde{u}_{i\alpha}) \right]^*, \quad (6)$$

where $\tilde{\bar{q}}$ denotes an anti-squark and the stars stand for complex conjugation. Note that even in a CP-conserving scenario some neutralino couplings have to be complex (more exactly, purely imaginary) if we insist on using positive neutralino masses in all propagators [18]. If CP is violated, all chargino, neutralino and gluino couplings may be complex. Finally, recall that a right-handed anti-quark is an $SU(2)$ doublet; its couplings are therefore related to those of left-handed quarks, and vice versa.

2.2.2 $d_i d_j \rightarrow \tilde{d}_{i\alpha} \tilde{d}_{j\beta}$

The process $d_i d_j \rightarrow \tilde{d}_{i\alpha} \tilde{d}_{j\beta}$ and its charge-conjugated process are given by Eqs.(3) to (6), with the obvious replacement $\tilde{u} \rightarrow \tilde{d}$ everywhere.

2.2.3 $u_i d_j \rightarrow \tilde{u}_{i\alpha} \tilde{d}_{j\beta}$

This process receives contributions from the t -channel exchange of a neutralino or gluino; if both (s)quarks are from the same generation, $i = j$, there is also a u -channel chargino exchange contribution. The corresponding Feynman diagrams are shown in Fig. 2.

The squared spin- and color-averaged matrix element is given by

$$\overline{|M|}^2 = \Phi(\tilde{u}_{i\alpha}, \tilde{d}_{j\beta}, 1) + \chi(\tilde{u}_{i\alpha}, \tilde{d}_{i\beta}, 2)\delta_{ij} + \Psi(\tilde{u}_{i\alpha}, \tilde{d}_{i\beta}, 3)\delta_{ij}. \quad (7)$$

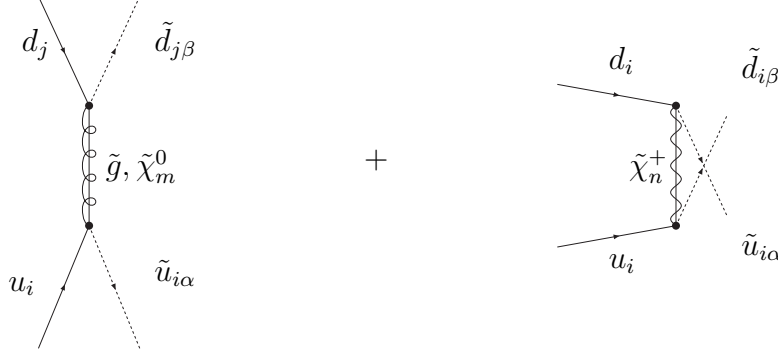


Figure 2: Feynman diagrams contributing to $u_i d_j \rightarrow \tilde{u}_{i\alpha} \tilde{d}_{j\beta}$. The notation in the t -channel diagram is as in Fig. 1. In the second, u -channel, diagram, which only exists of $i = j$, the chargino index n runs from 1 to 2.

The color factors for the squared t -channel neutralino and gluino contributions, squared u -channel chargino contributions and of the interference terms are given by

$$c_1(l, k) = \begin{pmatrix} 1 & 1 & 1 & 1 & 0 \\ 1 & 1 & 1 & 1 & 0 \\ 1 & 1 & 1 & 1 & 0 \\ 1 & 1 & 1 & 1 & 0 \\ 0 & 0 & 0 & 0 & 2/9 \end{pmatrix}, \quad c_2(l, k) = \begin{pmatrix} 1 & 1 \\ 1 & 1 \end{pmatrix}, \quad c_3(l, k) = \begin{pmatrix} 1 & 1 \\ 1 & 1 \\ 1 & 1 \\ 1 & 1 \\ 4/9 & 4/9 \end{pmatrix}. \quad (8)$$

In the squared t -channel diagrams the indices l, k labeling the exchanged particles run from 1 to 5 for the four neutralinos and gluino, whereas in the squared u -channel chargino-exchange contribution the indices run from 1 to 2. In the interference contribution the index l labeling the particle exchanged in the t -channel again runs from 1 to 5, while k takes the values 1 or 2. The couplings to be inserted in Eqs.(2) are given by

$$\begin{aligned} a(l, \tilde{u}_{i\alpha}) &= a_{\tilde{\chi}_l^0/\tilde{g}}(\tilde{u}_{i\alpha}), & b(l, \tilde{u}_{i\alpha}) &= b_{\tilde{\chi}_l^0/\tilde{g}}(\tilde{u}_{i\alpha}), \\ a'(l, \tilde{d}_{j\beta}) &= a_{\tilde{\chi}_l^0/\tilde{g}}(\tilde{d}_{j\beta}), & b'(l, \tilde{d}_{j\beta}) &= b_{\tilde{\chi}_l^0/\tilde{g}}(l, \tilde{d}_{j\beta}), \\ c(l, \tilde{d}_{i\beta}) &= a_{\tilde{\chi}_l^+}(\tilde{d}_{i\beta}), & d(l, \tilde{d}_{i\beta}) &= b_{\tilde{\chi}_l^+}(\tilde{d}_{i\beta}), \\ c'(l, \tilde{u}_{i\alpha}) &= a_{\tilde{\chi}_l^+}(\tilde{u}_{i\alpha}), & d'(l, \tilde{u}_{i\alpha}) &= b_{\tilde{\chi}_l^+}(\tilde{u}_{i\alpha}) \end{aligned} \quad (9)$$

The explicit expressions for the couplings appearing in Eqs.(9) can be found in Eqs.(30), (31) and (32) in the Appendix.

The cross section for the charge-conjugated process can again be obtained by using the appropriate couplings for anti-(s)quarks in Eqs.(2):

$$\begin{aligned} a_{\tilde{\chi}_l^0/\tilde{g}/\tilde{\chi}_l^+}(\bar{\tilde{d}}_{i\alpha}) &= \left[b_{\tilde{\chi}_l^0/\tilde{g}/\tilde{\chi}_l^+}(\tilde{d}_{i\alpha}) \right]^*, & b_{\tilde{\chi}_l^0/\tilde{g}/\tilde{\chi}_l^+}(\bar{\tilde{d}}_{i\alpha}) &= \left[a_{\tilde{\chi}_l^0/\tilde{g}/\tilde{\chi}_l^+}(\tilde{d}_{i\alpha}) \right]^*, \\ a_{\tilde{\chi}_l^0/\tilde{g}/\tilde{\chi}_l^+}(\bar{\tilde{u}}_{i\alpha}) &= \left[b_{\tilde{\chi}_l^0/\tilde{g}/\tilde{\chi}_l^+}(\tilde{u}_{i\alpha}) \right]^*, & b_{\tilde{\chi}_l^0/\tilde{g}/\tilde{\chi}_l^+}(\bar{\tilde{u}}_{i\alpha}) &= \left[a_{\tilde{\chi}_l^0/\tilde{g}/\tilde{\chi}_l^+}(\tilde{u}_{i\alpha}) \right]^*. \end{aligned} \quad (10)$$

2.2.4 $u_i d_j \rightarrow \tilde{d}_{i\alpha} \tilde{u}_{j\beta}$, $i \neq j$

This process differs from the one considered in the previous subsection only if the two (s)quarks are from *different* generation, with the d -type squark in the final state being from the same generation as the initial u -type quark. In this case only the chargino exchange diagram shown in Fig. 3 contributes. We label the momenta such that this is a t -channel diagram.

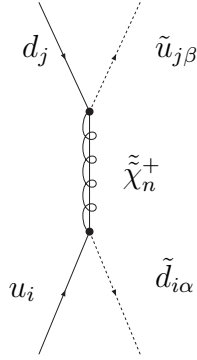


Figure 3: Feynman diagram contributing to $u_i d_j \rightarrow \tilde{u}_{j\alpha} \tilde{d}_{i\beta}$ with $i \neq j$. The notation is as in the chargino exchange diagram of Fig. 2.

The squared spin- and color-averaged matrix element is given by

$$|\overline{M}|^2 = \Phi(\tilde{d}_{i\alpha}, \tilde{u}_{j\beta}, 1). \quad (11)$$

The colour factor is trivial,

$$c_1 = \begin{pmatrix} 1 & 1 \\ 1 & 1 \end{pmatrix}. \quad (12)$$

The couplings to be inserted in Eqs.(2) are,

$$\begin{aligned} a(l, \tilde{d}_{i\alpha}) &= a_{\tilde{\chi}_l^+}(\tilde{d}_{i\alpha}), & b(l, \tilde{d}_{i\alpha}) &= b_{\tilde{\chi}_l^+}(\tilde{d}_{i\alpha}), \\ a'(l, \tilde{u}_{j\beta}) &= a_{\tilde{\chi}_l^+}(\tilde{u}_{j\beta}), & b'(l, \tilde{u}_{j\beta}) &= b_{\tilde{\chi}_l^+}(\tilde{u}_{j\beta}) \end{aligned} \quad (13)$$

The cross section for the charge conjugated process can be obtained by using the appropriate anti-(s)quark couplings, which have already been given in Eqs.(10).

2.3 $q\bar{q}' \rightarrow \tilde{q}\tilde{\bar{q}}$

We now turn to processes with one squark and one anti-squark in the final state. Since now the initial and final state have vanishing baryon charge, s -channel diagrams may contribute.

2.3.1 $u_i \bar{u}_j \rightarrow \tilde{u}_{i\alpha} \bar{\tilde{u}}_{j\beta}$

This process receives contributions from the exchange of a gluino or neutralino in the t -channel; if $i = j$, there are also s -channel gluon, photon and Z exchange contributions. The corresponding Feynman diagrams are shown in Fig. 4.

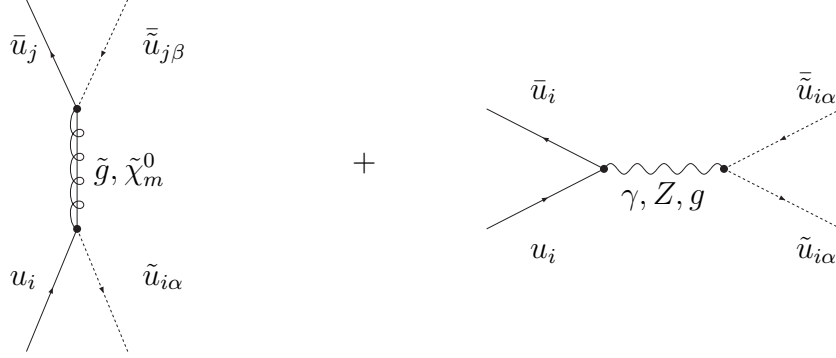


Figure 4: Feynman diagrams contributing to $u_i \bar{u}_j \rightarrow \tilde{u}_{i\alpha} \bar{\tilde{u}}_{j\beta}$. The notation for the t -channel diagram is as in Fig.1. The gauge boson exchanged in the second, s -channel, diagram, which only exists if $i = j$, can be a gluon, a photon or a Z boson.

The squared spin- and color-averaged matrix element is given by

$$\overline{|M|}^2 = \Phi(\tilde{u}_{i\alpha}, \bar{\tilde{u}}_{j\beta}, 1) + \Upsilon(u_i, \bar{u}_i, \tilde{u}_{i\alpha}, \bar{\tilde{u}}_{i\alpha}, 2)\delta_{ij}\delta_{\alpha\beta} + \Omega(u_i, \bar{u}_i, \tilde{u}_{i\alpha}, \bar{\tilde{u}}_{i\alpha}, 3)\delta_{ij}\delta_{\alpha\beta}. \quad (14)$$

The color factors of the pure t -channel neutralino and gluino contributions, the s -channel γ, Z , gluon contributions and the interference terms are given by

$$\begin{aligned} c_1(l, k) &= \begin{pmatrix} 1 & 1 & 1 & 1 & 0 \\ 1 & 1 & 1 & 1 & 0 \\ 1 & 1 & 1 & 1 & 0 \\ 1 & 1 & 1 & 1 & 0 \\ 0 & 0 & 0 & 0 & 2/9 \end{pmatrix}, & c_2(l, k) &= \begin{pmatrix} 1 & 1 & 0 \\ 1 & 1 & 0 \\ 0 & 0 & 2/9 \end{pmatrix}, \\ c_3(l, k) &= \begin{pmatrix} 1 & 1 & 1 & 1 & 4/9 \\ 1 & 1 & 1 & 1 & 4/9 \\ 4/9 & 4/9 & 4/9 & 4/9 & -2/27 \end{pmatrix}. \end{aligned} \quad (15)$$

The couplings to be inserted in Eqs.(2) are given by:

$$\begin{aligned} a(l, \tilde{u}_{i\alpha}) &= a_{\tilde{\chi}_l^0/\tilde{g}}(\tilde{u}_{i\alpha}), & b(l, \tilde{u}_{i\alpha}) &= b_{\tilde{\chi}_l^0/\tilde{g}}(\tilde{u}_{i\alpha}), \\ a'(l, \bar{\tilde{u}}_{j\beta}) &= [b_{\tilde{\chi}_l^0/\tilde{g}}(\tilde{u}_{j\beta})]^*, & b'(l, \bar{\tilde{u}}_{j\beta}) &= [a_{\tilde{\chi}_l^0/\tilde{g}}(\tilde{u}_{j\beta})]^*, \\ e(l, u_i, \bar{u}_i) &= e_{\gamma/Z/g}(u_i, \bar{u}_i), & f(l, u_i, \bar{u}_i) &= q_{\gamma/Z/g}(u_i, \bar{u}_i), \\ c(l, \tilde{u}_{i\alpha}, \bar{\tilde{u}}_{i\alpha}) &= c_{\gamma/Z/g}(\tilde{u}_{i\alpha}, \bar{\tilde{u}}_{i\alpha}). \end{aligned} \quad (16)$$

Recall that in s -channel diagrams $l = 1$ stands for a photon, $l = 2$ for a Z -boson, and $l = 3$ for a gluon. The explicit expressions for the couplings of these gauge bosons can be found in Eqs.(33) and (34) in the Appendix.

2.3.2 $u_i \bar{u}_i \rightarrow \tilde{q}_{j\alpha} \tilde{\bar{q}}_{j\alpha}, \quad i \neq j$

Since the flavor in the initial and final state is different, only the s -channel diagrams of Fig.4 contribute. The squared spin- and color-averaged matrix element is thus simply given by

$$\overline{|M|}^2 = \Upsilon(u_i, \bar{u}_i, \tilde{q}_{i\alpha}, \tilde{\bar{q}}_{i\alpha}, 1). \quad (17)$$

The colour factors are

$$c_1(l, k) = \begin{pmatrix} 1 & 1 & 0 \\ 1 & 1 & 0 \\ 0 & 0 & 2/9 \end{pmatrix}. \quad (18)$$

The couplings to be inserted in Eqs.(2) can be read off from Eqs.(16).

2.3.3 $u_i \bar{u}_j \rightarrow \tilde{d}_{i\alpha} \tilde{\bar{d}}_{j\beta}$

This process receives contributions from chargino exchange in the t -channel; if $i = j$, there are also s -channel contributions with gluon, photon and Z -exchange. The corresponding Feynman diagrams are shown in Fig. 5.

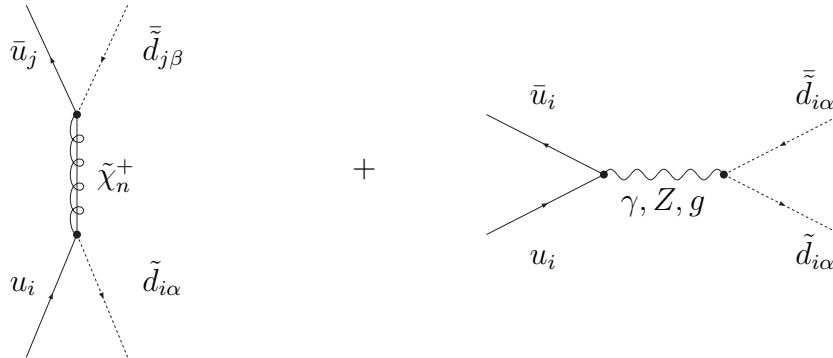


Figure 5: Feynman diagrams contributing to $u_i \bar{u}_j \rightarrow \tilde{d}_{i\alpha} \tilde{\bar{d}}_{j\beta}$. The notation for the t -channel diagram is as in Fig.3. The notation for the second, s -channel, diagram, which only exists if $i = j$, is as in Fig. 4.

The squared spin- and color-averaged matrix element is given by

$$\overline{|M|}^2 = \Phi(\tilde{d}_{i\alpha}, \tilde{\bar{d}}_{j\beta}, 1) + \Upsilon(u_i, \bar{u}_i, \tilde{d}_{i\alpha}, \tilde{\bar{d}}_{i\alpha}, 2) \delta_{ij} \delta_{\alpha\beta} + \Omega(u_i, \bar{u}_i, \tilde{d}_{i\alpha}, \tilde{\bar{d}}_{i\alpha}, 3) \delta_{ij} \delta_{\alpha\beta}. \quad (19)$$

The respective colour factors for the squared t -channel, squared s -channel and the interference terms are given by

$$c_1 = \begin{pmatrix} 1 & 1 \\ 1 & 1 \end{pmatrix}, \quad c_2(l, k) = \begin{pmatrix} 1 & 1 & 0 \\ 1 & 1 & 0 \\ 0 & 0 & 2/9 \end{pmatrix}, \quad c_3(l, k) = \begin{pmatrix} 1 & 1 \\ 1 & 1 \\ 4/9 & 4/9 \end{pmatrix}. \quad (20)$$

The couplings to be inserted in Eqs.(2) are given by

$$\begin{aligned} a(l, \tilde{d}_{i\alpha}) &= a_{\tilde{\chi}_l^+}(\tilde{d}_{i\alpha}), & a'(l, \tilde{d}_{j\beta}) &= [b_{\tilde{\chi}_l^+}(\tilde{d}_{j\beta})]^*, \\ b(l, \tilde{d}_{i\alpha}) &= b_{\tilde{\chi}_l^+}(\tilde{d}_{i\alpha}), & b'(l, \tilde{d}_{j\beta}) &= [a_{\tilde{\chi}_l^+}(\tilde{d}_{j\beta})]^*, \\ e(l, u_i, \bar{u}_i) &= e_{\gamma/Z/g}(u_i, \bar{u}_i), & f(l, u_i, \bar{u}_i) &= q_{\gamma/Z/g}(u_i, \bar{u}_i), \\ c(l, \tilde{d}_{i\alpha}, \tilde{\bar{d}}_{i\alpha}) &= c_{\gamma/Z/g}(\tilde{d}_{i\alpha}, \tilde{\bar{d}}_{i\alpha}). \end{aligned} \quad (21)$$

2.3.4 $d_i \bar{d}_j \rightarrow \tilde{q} \tilde{\bar{q}}$

Each of the last three processes has an analogue where all u -type (s)quarks are replaced by d -type (s)quarks and vice versa. The cross sections for these reactions can be described by simply replacing $u \rightarrow d$ and $d \rightarrow u$ everywhere.

2.3.5 $d_i \bar{u}_j \rightarrow \tilde{d}_{i\alpha} \tilde{\bar{u}}_{j\beta}$

This process receives contributions from the exchange of a gluino or neutralino in the t -channel; if $i = j$, there is also an s -channel W exchange contribution. The corresponding Feynman diagrams are shown in Fig. 6.

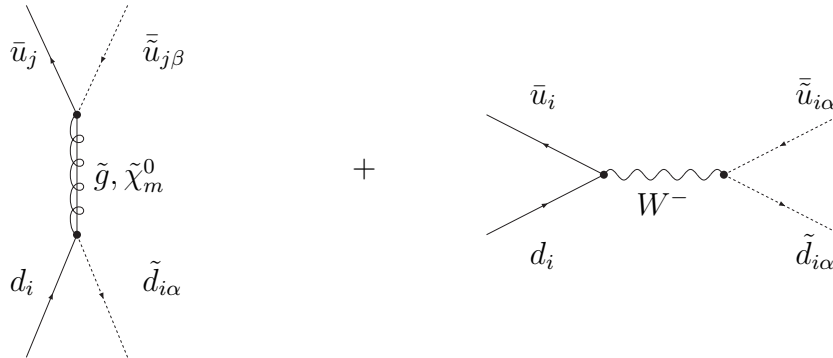


Figure 6: Feynman diagrams contributing to $d_i \bar{u}_j \rightarrow \tilde{d}_{i\alpha} \tilde{\bar{u}}_{j\beta}$. The notation for the t -channel diagram is as in Fig.3. The second, s -channel, diagram, which only exists if $i = j$, proceeds via the exchange of a charged W boson.

The squared spin- and color-averaged matrix element is given by

$$|\overline{M}|^2 = \Phi(\tilde{d}_{i\alpha}, \tilde{u}_{j\beta}, 1) + \Upsilon(d_i, \bar{u}_i, \tilde{d}_{i\alpha}, \tilde{u}_{i\alpha}, 2)\delta_{ij}\delta_{\alpha\beta} + \Omega(d_i, \bar{u}_i, \tilde{d}_{i\alpha}, \tilde{u}_{i\alpha}, 3)\delta_{ij}\delta_{\alpha\beta}. \quad (22)$$

The color factors for the pure t -channel, pure s -channel and interference terms are

$$c_1(l, k) = \begin{pmatrix} 1 & 1 & 1 & 1 & 0 \\ 1 & 1 & 1 & 1 & 0 \\ 1 & 1 & 1 & 1 & 0 \\ 1 & 1 & 1 & 1 & 0 \\ 0 & 0 & 0 & 0 & 2/9 \end{pmatrix}, \quad c_2 = 1, \quad c_3 = \begin{pmatrix} 1 & 1 & 1 & 1 & 4/9 \end{pmatrix}. \quad (23)$$

The couplings to be inserted in Eqs.(2) are

$$\begin{aligned} a(l, \tilde{d}_{i\alpha}) &= a_{\tilde{\chi}_l^0/\tilde{g}}(\tilde{d}_{i\alpha}), & a'(l, \tilde{u}_{j\beta}) &= \left[b_{\tilde{\chi}_l^0/\tilde{g}}(\tilde{u}_{j\beta}) \right]^*, \\ b(l, \tilde{d}_{i\alpha}) &= b_{\tilde{\chi}_l^0/\tilde{g}}(\tilde{d}_{i\alpha}), & b'(l, \tilde{u}_{j\beta}) &= \left[a_{\tilde{\chi}_l^0/\tilde{g}}(\tilde{u}_{j\beta}) \right]^*, \\ e(d_i, \bar{u}_i) &= e_W(d_i, \bar{u}_i), & f(d_i, \bar{u}_i) &= f_W(l, d_i, \bar{u}_i), \\ c(l, \tilde{d}_{i\alpha}, \tilde{u}_{i\alpha}) &= c_W(\tilde{d}_{i\alpha}, \tilde{u}_{i\alpha}) \end{aligned} \quad (24)$$

Explicit expressions for the couplings of the W boson can be found in Eqs.(35) and (36) in the Appendix.

Unlike for the processes discussed so far in this Subsection, charge conjugation here leads to a physically different reaction. The cross section for this process can be obtained from Eqs.(22)–(24) by replacing (s)quark couplings with anti-(s)quark couplings and vice versa. The new couplings appearing in the t -channel diagrams can e.g. be read off from Eqs.(10), whereas the couplings in the s -channel diagram remain unchanged.

2.3.6 $d_i \bar{u}_i \rightarrow \tilde{d}_{j\alpha} \tilde{u}_{j\beta}, \quad i \neq j$

This process can only proceed through the exchange of a charged W boson in the s -channel. The corresponding Feynman diagram has already been shown in Fig. 6. The squared spin- and color-averaged matrix element is simply given by

$$|\overline{M}|^2 = \Upsilon(d_i, \bar{u}_i, \tilde{d}_{j\alpha}, \tilde{u}_{j\beta}, 1). \quad (25)$$

The color factor is trivial, $c_1 = 1$. The couplings to be inserted in Eqs.(2) are

$$\begin{aligned} e(l, d_i, \bar{u}_i) &= e_W(d_i, \bar{u}_i), & f(l, d_i, \bar{u}_i) &= f_W(l, d_i, \bar{u}_i), \\ c(l, \tilde{d}_{j\alpha}, \tilde{u}_{j\beta}) &= c_W(\tilde{d}_{j\alpha}, \tilde{u}_{j\beta}). \end{aligned} \quad (26)$$

The squared matrix element for the charge conjugated process is identical.

3 Numerical Results

We are now ready to present numerical results. We focus on pp collisions at the LHC operating at $\sqrt{s} = 14$ TeV, since in most predictive models of supersymmetry breaking [1] the existing

Scenario	m_0	$m_{1/2}$	$m_{\tilde{q}}$	QCD		QCD + EW		ratio	
				Total	LL	Total	LL	Total	LL
SPS 1a	100	250	560	12.11	3.09	12.55	3.50	1.036	1.133
SPS 1b	200	400	865	1.57	0.42	1.66	0.499	1.055	1.186
SPS 2	1450	300	1590	0.0553	0.0132	0.0567	0.0144	1.025	1.091
SPS 3	90	400	845	1.74	0.464	1.83	0.551	1.055	1.188
SPS 4	400	300	760	3.10	0.813	3.22	0.927	1.040	1.141
SPS 5	150	300	670	5.42	1.41	5.66	1.62	1.042	1.152

Table 1: Total cross sections at the LHC for combined first and second generation squark pair production from quark initial states in six mSUGRA benchmark scenarios. All masses are in GeV, m_0 and $m_{1/2}$ being the common soft breaking scalar and gaugino masses, respectively, at the scale of Grand Unification, and $m_{\tilde{q}}$ giving the average mass of first generation $SU(2)$ doublet squarks. All cross sections are in pb. The last two columns show the ratio (QCD + EW) / QCD. We show results for the sum over all squark pairs (“total”), as well as for the sum over all combinations of two $SU(2)$ doublet squarks (“LL”); in both cases we include squarks and anti-squarks. The cross sections have been calculated in leading order, using the CTEQ5L parton distribution functions [20].

bounds [19] on the masses of sleptons and charginos imply that first and second generation squarks are too heavy to be produced at the Tevatron. Since our calculation is leading order in QCD, we use CTEQ5L structure functions [20], as well as the one-loop expression for the running QCD coupling α_s , with five active flavors and $\Lambda_{\text{QCD}} = 142$ MeV. The electroweak gauge couplings, as well as the relevant superparticle masses, are taken from the output of the program package SoftSUSY [21]. The couplings are $\overline{\text{MS}}$ couplings at a scale near the squark masses, whereas the squark and gluino masses are on-shell (pole) masses. We focus on squarks of the first and second generation, where mixing between $SU(2)$ doublets and singlets can be neglected. Third generation squarks are produced dominantly through gluon fusion or pure s -channel diagrams; the EW contributions to these cross sections will therefore be very small. Experimentally the production of third generation squarks can be distinguished by detecting b or t quarks in the final state.

Table 1 shows results for the total squark pair production cross sections at the LHC in six mSUGRA benchmark scenarios, taken from [14]. Here we sum over all squarks and anti-squarks of the first and second generation; results where both final state (anti-)squarks are $SU(2)$ doublets are shown separately. We only include contributions with (anti-)quarks in the initial state, since the gluon fusion contribution obviously does not receive electroweak contributions in leading order. Besides, the gluon fusion contribution is subdominant in all cases; it increases the QCD contribution by 14 (6.7, 1.4)% for SPS 1a (1b, 2).³ We take equal factorization and renormalization scales, $\mu_F = \mu_R = m_{\tilde{q}}/2$; this choice leads to quite small NLO corrections to the pure QCD contribution [12]. Increasing (reducing) these scales will reduce (increase) the prediction for the pure QCD contribution, thereby enhancing (diminishing) the relative importance of the electroweak contributions.

³The *inclusive* squark production cross section also receives large contributions from associate $\tilde{q}\tilde{g}$ production from pure QCD, as well as from $\tilde{q}\tilde{\chi}^{\pm,0}$ production at $\mathcal{O}(\alpha_s\alpha_w)$ [11].

Not surprisingly, the cross sections fall quickly with increasing squark mass. The partonic cross sections scale like $m_{\tilde{q}}^{-2}$, if the ratios of sparticle masses are kept fixed and the running of α_s is ignored. In addition, the pdf factors decrease quickly with increasing squark mass. There is also some dependence on the gluino mass ($\simeq 2.5m_{1/2}$), which appears in t - and u -channel propagators. Varying the ratio $m_{\tilde{g}}/m_{\tilde{q}}$ between 0.5 and 1.2, which is the range covered by the scenarios of Table 1, leads to 15 to 20% variation of the QCD prediction. We will discuss the gaugino mass dependence in more detail later.

Since QCD contributions dominate even after inclusion of the electroweak diagrams, the overall behavior of the total cross sections does not change much. These contributions are clearly more important for the production of $SU(2)$ doublet squarks than for the total cross section summed over all final states. This is not surprising: the cross sections for all other combinations of squarks only receive electroweak contributions due to hypercharge interactions, and the squared $SU(2)$ gauge coupling exceeds the squared $U(1)_Y$ coupling by a factor $\cot^2 \theta_W \simeq 3.3$.

However, the weakness of the $U(1)_Y$ coupling by itself is not sufficient to explain the small size of electroweak contributions to final states involving at least one $SU(2)$ singlet (anti-)squark. For example, we can infer from the first line of Table 1 that in scenario SPS 1a, electroweak contributions increase the cross section for the production of two L -type squarks by 0.41 pb, whereas they only contribute 0.03 pb to all other squark pair production channels combined. We also note that the importance of the EW contributions seems to depend much more strongly on the ratio $m_{1/2}/m_0$ than the QCD prediction does. Finally, the EW contributions evidently become more important for heavier squarks if the ratio $m_0/m_{1/2}$ remains roughly the same.

In order to understand these features, in Table 2 we list results for all 24 different processes involving only (s)quarks and anti-(s)quarks from the first generation. These results are for SPS 1a, but we find similar patterns in the other scenarios.

These 24 processes can be grouped into three categories. The first seven reactions show interference between t - and u -channel diagrams, where in all but the last case there are both strong and electroweak contributions from both t - and u -channel diagrams. The next class of seven processes allows interference between s - and t -channel diagrams. In the first four cases there are both QCD and electroweak contributions to both the t - and s -channel, while in the last three cases only one QCD diagram contributes. For the third class of ten processes, no interference between electroweak and strong contributions is possible; two of these processes only proceed via s -channel diagrams, whereas the remaining eight are pure t -channel reactions.

Within processes proceeding through t - or u -channel diagrams, it is important to distinguish between reactions that require a helicity flip of the exchanged fermion, and those that don't. Consider reactions with two squarks with equal 'chirality' in the final state, e.g. $\tilde{u}_L \tilde{u}_L$ production (process no. 1 in Table 2). In this case both quarks in the initial state have to be left-handed, since the quark-squark-gaugino gauge couplings couple L -type squarks only to left-handed quarks. This evidently requires a helicity flip of the exchanged gaugino, i.e. the corresponding amplitudes are proportional to the mass of the exchanged gaugino. In models with gaugino mass unification this further suppresses electroweak contributions in this important class of processes, since the $SU(2)$ and $U(1)_Y$ gaugino masses are respectively three and six times smaller than the gluino mass. On the other hand, the equal helicities in the initial state imply that total angular momentum $J = 0$, so that the produced squarks can be in an

S -wave. The cross section therefore receives only a single power of the threshold factor β (which is the squark center-of-mass [cms] velocity).

In contrast, the production of one L -type and one R -type squark, e.g. $\tilde{u}_L\tilde{u}_R$ production (process no. 3 in Table 2), requires *opposite* helicities of the two initial quarks. The exchanged fermion therefore does not need to change helicity, i.e. these amplitudes remain finite even in the limit of vanishing gaugino masses. On the other hand, now both quark spins point in the same direction, so that $J = 1$. The produced squarks therefore have to be in a P -wave, resulting in a cross section that is suppressed by two additional powers of β relative to S -wave reactions. Notice that for the purpose of this distinction an R -type anti-squark acts like an L -type squark, since it couples to a left-handed particle $[\overline{q}_R = (\bar{q})_L]$; similarly, an L -type anti-squark acts like an R -type squark. Finally, pure s -channel processes also require the squarks to be in a P -wave, i.e. have cross sections $\propto \beta^3$.

With this understanding, let us come back to Table 2 and its three categories of reactions. In the first category the electroweak contributions almost always increase the cross section. The exception is $dd \rightarrow \tilde{d}_L\tilde{d}_R$, where the interference term is negative; however, due to the small hypercharges involved, the electroweak contribution is very small in this case. In fact, as argued above, electroweak contributions are sizable only if both produced squarks are $SU(2)$ doublets, although owing to the large hypercharge the electroweak contribution to the $\tilde{u}_R\tilde{u}_R$ final state is not completely negligible. The biggest electroweak contribution occurs in $ud \rightarrow \tilde{u}_L\tilde{d}_L$. Here the gluino t -channel contribution interferes with a chargino u -channel contribution; in the limit where one of the charginos is a pure $SU(2)$ gaugino (charged wino), its couplings to a quark and a squark exceed those of the corresponding neutralino by a factor $\sqrt{2}$. One might therefore expect the electroweak contributions to this channel to be twice as important as for $\tilde{u}_L\tilde{u}_L$ or $\tilde{d}_L\tilde{d}_L$ production. Table 2 shows that the actual enhancement factor is somewhat smaller than this. The reason is that the relative importance of the electroweak contributions to $\tilde{u}_L\tilde{u}_L$ and $\tilde{d}_L\tilde{d}_L$ production is enhanced by the destructive interference between the two QCD gluino (t - and u -channel) diagrams.

Note that all reactions in this category that can proceed via $SU(2)$ interactions require a helicity flip. In models with gaugino mass unification the EW contributions are therefore significantly smaller than a naive guess based on coupling constants only; this is only partly compensated by the fact that the color factor for the interference terms is two times bigger than for the pure QCD amplitudes, see e.g. Eq.(4).

The different absolute sizes of the total cross sections for these seven reactions are determined by the interplay of four effects. Cross sections for the production of two identical particles in the final state are suppressed by the statistics factor $1/2$. On the other hand, we saw above that $\tilde{u}_L\tilde{u}_R$ and $\tilde{d}_L\tilde{d}_R$ production can only occur in a P (or higher) partial wave; the resulting cross sections are therefore suppressed by an extra factor of β^2 . In the given scenario this gives a similar suppression as the statistics factor for producing two equal squarks; if squarks are heavier, this threshold suppression over-compensates the statistics factor. Note also that the flux of valence u -quarks in the proton is very roughly two times larger than that of valence d -quarks. The ratio of the two pdf's increases with increasing Bjorken- x ; the preponderance of \tilde{u} over \tilde{d} squarks therefore becomes more prominent for larger squark masses. Finally, in mSUGRA $SU(2)$ doublet squarks are somewhat heavier than their $SU(2)$ singlet counterparts, since the masses of the latter are not enhanced by $SU(2)$ gaugino loop contributions. The pure QCD cross section for $SU(2)$ -singlets is therefore somewhat bigger than that for doublets.

No.	Process	diagrams		helicity flip?	thre- shold	cross section [pb]		ratio
		QCD	EW			QCD	QCD + EW	
1	$uu \rightarrow \tilde{u}_L \tilde{u}_L$	t, u	t, u	yes	β	0.683	0.794	1.162
2	$uu \rightarrow \tilde{u}_R \tilde{u}_R$	t, u	t, u	yes	β	0.761	0.796	1.045
3	$uu \rightarrow \tilde{u}_L \tilde{u}_R$	t, u	t, u	no	β^3	0.929	0.931	1.002
4	$dd \rightarrow \tilde{d}_L \tilde{d}_L$	t, u	t, u	yes	β	0.198	0.232	1.171
5	$dd \rightarrow \tilde{d}_R \tilde{d}_R$	t, u	t, u	yes	β	0.234	0.237	1.012
6	$dd \rightarrow \tilde{d}_L \tilde{d}_R$	t, u	t, u	no	β^3	0.243	0.243	1.000
7	$ud \rightarrow \tilde{u}_L \tilde{d}_L$	t	t, u	yes	β	0.969	1.22	1.261
8	$u\bar{u} \rightarrow \tilde{u}_L \tilde{u}_L$	s, t	s, t	no	β^3	0.165	0.140	0.848
9	$u\bar{u} \rightarrow \tilde{u}_R \tilde{u}_R$	s, t	s, t	no	β^3	0.187	0.170	0.909
10	$d\bar{d} \rightarrow \tilde{d}_L \tilde{d}_L$	s, t	s, t	no	β^3	0.0925	0.0784	0.847
11	$d\bar{d} \rightarrow \tilde{d}_R \tilde{d}_R$	s, t	s, t	no	β^3	0.109	0.106	0.972
12	$u\bar{u} \rightarrow \tilde{d}_L \tilde{d}_L$	s	s, t	no	β^3	0.0341	0.0353	1.035
13	$d\bar{d} \rightarrow \tilde{u}_L \tilde{u}_L$	s	s, t	no	β^3	0.0207	0.0219	1.057
14	$u\bar{d} \rightarrow \tilde{u}_L \tilde{d}_L$	t	s, t	no	β^3	0.178	0.162	0.910
15	$ud \rightarrow \tilde{u}_L \tilde{d}_R$	t	t	no	β^3	0.484	0.485	1.001
16	$ud \rightarrow \tilde{u}_R \tilde{d}_L$	t	t	no	β^3	0.477	0.479	1.002
17	$ud \rightarrow \tilde{u}_R \tilde{d}_R$	t	t	yes	β	1.113	1.114	1.001
18	$u\bar{u} \rightarrow \tilde{u}_L \tilde{u}_R$	t	t	yes	β	0.569	0.569	1.000
19	$d\bar{d} \rightarrow \tilde{d}_L \tilde{d}_R$	t	t	yes	β	0.331	0.331	1.000
20	$u\bar{d} \rightarrow \tilde{u}_L \tilde{d}_R$	t	t	yes	β	0.491	0.491	1.000
21	$u\bar{d} \rightarrow \tilde{u}_R \tilde{d}_L$	t	t	yes	β	0.480	0.480	1.000
22	$u\bar{d} \rightarrow \tilde{u}_R \tilde{d}_R$	t	t	no	β^3	0.202	0.203	1.004
23	$u\bar{u} \rightarrow \tilde{d}_R \tilde{d}_R$	s	s	—	β^3	0.0420	0.0421	1.002
24	$d\bar{d} \rightarrow \tilde{u}_R \tilde{u}_R$	s	s	—	β^3	0.0240	0.0240	1.000

Table 2: The 24 different squark pair production processes involving first generation (s)quarks only; charge conjugate reactions are included in the cross section if they differ from the listed ones. The letters s, t, u stand for the existence of s -, t - and u -channel diagrams, respectively; this is listed separately for strong and electroweak interactions. We also list whether the exchange of a fermion in the t - and/or u -channel requires a helicity flip. The fifth column describes the threshold behavior of the cross section, in terms of the squark velocity β in the center-of-mass frame; a behavior $\propto \beta$ (β^3) indicates an S - (P -)wave cross section. The values of the cross sections are for scenario SPS 1a (see Table 1). The last column shows the relative size of the electroweak contributions.

However, this difference is largely canceled by the electroweak contributions, which, as we just saw, are much more important for the doublets.

All seven reactions in the second category of Table 2 require an anti-quark in the initial state; moreover, all cross sections suffer from P -wave suppression. They are therefore substantially

smaller than the cross sections in the first group; this difference becomes even bigger for larger squark masses. On the other hand, since the \bar{u} and \bar{d} densities in the proton are similar, the cross sections for processes with u quarks in the initial state are now only about two times larger than those with d -quarks.

More important for our purposes is that for most of these processes, electroweak contributions *reduce* the total cross section. This is because both the interference between QCD s -channel and EW t -channel diagrams, and that between QCD t -channel and EW s -channel diagrams is *destructive* for all these seven processes.⁴ This effect is most prominent for $q\bar{q} \rightarrow \tilde{q}_L \tilde{q}_L$ ($q = u, d$), where the dominant EW contribution is due to $SU(2)$ gauge interactions. However, the EW contribution is also sizable for $u\bar{u} \rightarrow \tilde{u}_R \tilde{u}_R$, due to the relatively large hypercharges of the involved (s)quarks; recall that the $SU(2)$ neutralino coupling gets a factor $1/2$ from weak isospin, which is smaller than the hypercharge of the right-handed u -quark and its superpartner. These processes do not require a helicity flip, i.e. there is no factor of the mass of the exchanged fermion in the t -channel amplitudes. The t -channel propagators then favor the lightest exchanged fermion. This enhances the EW contributions relative to the QCD ones, and the $U(1)$ contribution relative to the one due to $SU(2)$ interactions. The relatively mild suppression of the $\tilde{u}_L \tilde{d}_L$ final state, which is also accessible via $SU(2)$ interactions, can be explained from the observation that here no QCD s -channel diagram contributes. This reduces the number of interference terms, but does not change the pure QCD contribution much, since here s -channel diagrams are subdominant.

Finally, $u\bar{u} \rightarrow \tilde{d}_L \tilde{d}_L$ and $d\bar{d} \rightarrow \tilde{u}_L \tilde{u}_L$ can proceed in QCD only through s -channel diagrams, but receive EW contributions from t -channel (chargino exchange) diagrams. The interference between these diagrams is again destructive. However, for these reactions this is over-compensated by the squared EW t -channel contribution. The absence of QCD t -channel diagrams makes the pure QCD and interference contributions quite small. On the other hand, the factor $\sqrt{2}$ in each chargino coupling relative to the $SU(2)$ neutralino coupling enhances the pure EW t -channel contribution. For the case at hand, the pure QCD, pure EW and interference contributions are of roughly equal absolute size; nevertheless, because of the strong cancellation between the pure electroweak and interference contributions, the total effect of the EW contributions only amounts to a few percent. The total cross sections for these processes therefore remain very small.

In the ten cases of the third category, which does not allow interference between EW and QCD diagrams, the electroweak contributions are obviously always positive, but very small. This is largely due to the fact that all these reactions involve at least one $SU(2)$ singlet in the final state, so that only $U(1)_Y$ interactions contribute. On the other hand, the cross sections for the first eight (t -channel) processes are sizable; in fact, $\tilde{u}_R \tilde{d}_R$ production is one of the most important channels also for heavy squarks, since it can proceed from two valence quarks in the initial state, and allows an S -wave in the final state.

This discussion allows us to understand the small total size of EW contributions due to hypercharge interactions. The processes of the first category, which have relatively large cross sections, receive small, positive corrections. In the second category we find (relatively) bigger,

⁴The relevant products of couplings, as well as the color factors, are positive; however, the remainder of the function Ω defined in Eq.(2) is negative. On the other hand, QCD s - and t -channel diagrams, where present, interfere constructively, due to an additional sign provided by the color factor, see e.e. Eq.(15).

negative corrections, but the cross sections are smaller; the total contribution from $U(1)_Y$ interactions therefore remains positive. The relative importance of these contributions is further reduced by the large number of processes that receive only very small EW contributions, due to the absence of interference with QCD diagrams and/or due to the small hypercharges of the involved (s)quarks.

Coming back to Table 1, we saw that the relative importance of the electroweak contributions increases with increasing gaugino to squark mass ratio. This can be explained from our earlier observation that the most important EW contributions involve the interference of t - and u -channel amplitudes (category 1 in Table 2). As explained above, the amplitudes for all processes of this kind that receive contributions from $SU(2)$ interactions are proportional to a gaugino mass. These contributions are therefore sensitive to the ratio of gaugino and squark masses. In mSUGRA the relative importance of the EW contributions becomes largely insensitive to $m_{1/2}$ (for fixed squark mass) once $m_{1/2} \gtrsim m_0$. The physical squark masses are then essentially independent of m_0 , i.e. $m_{\tilde{q}} \propto m_{1/2}$, so that the ratios of gaugino and squark masses become independent of $m_{1/2}$. The situation might be different in models without gaugino mass unification; we will come back to this point shortly.

Finally, Table 1 also shows that the electroweak contributions become relatively more important with increasing squark mass scale, although for scenario SPS 2 this effect is overcompensated by the small ratio $m_{1/2}/m_0$. Table 2 shows that nine out of the ten processes where no interference occurs are suppressed by additional powers of the squark velocity β in the partonic cms frame, and/or by the presence of an anti-quark in the initial state. Increasing the squark mass reduces the amount of available phase space, i.e. the average β is reduced. Moreover, larger values of Bjorken- x are required, which reduces the flux of anti-quarks much more strongly than that of quarks. For the group of five processes with interference between s - and t -channel diagrams where electroweak contributions decrease the total cross section both suppression factors are present. The relative importance of these processes therefore decreases quickly with increasing squark mass. In contrast, the category 1 processes which receive large, positive EW contributions all receive contributions from two valence quarks in the initial state, and can have the squarks in an S -wave. Increasing the squark masses therefore enhances the relative importance of these processes.

We emphasized above that the dominant EW contributions come from the interference of t - and u -channel diagrams with QCD diagrams. Since in mSUGRA the electroweak gauginos are about three and six times lighter than the gluino, one expects the EW contributions to be most prominent for small transverse momenta of the produced squarks. This is borne out by Fig. 7, which shows the ratio of the tree-level differential cross section with and without EW contributions. Here, and in the subsequent figures, we concentrate on the production of two $SU(2)$ doublet (anti-)squarks, where the EW contributions are largest.

The observed behavior can be understood from the interplay of several effects. For simplicity assuming equal squark masses in the final state, the relation between the partonic cms energy and squark transverse momentum can be written as

$$\hat{s} = 4 \left(m_{\tilde{q}}^2 + \frac{p_T^2}{\sin^2 \theta} \right), \quad (27)$$

where θ is the cms scattering angle. The parton flux in the initial state is largest for smallest \hat{s} . Eq.(27) then shows that configurations where $\sin^2 \theta$ is maximal, i.e. where $\cos \theta$ is small, are

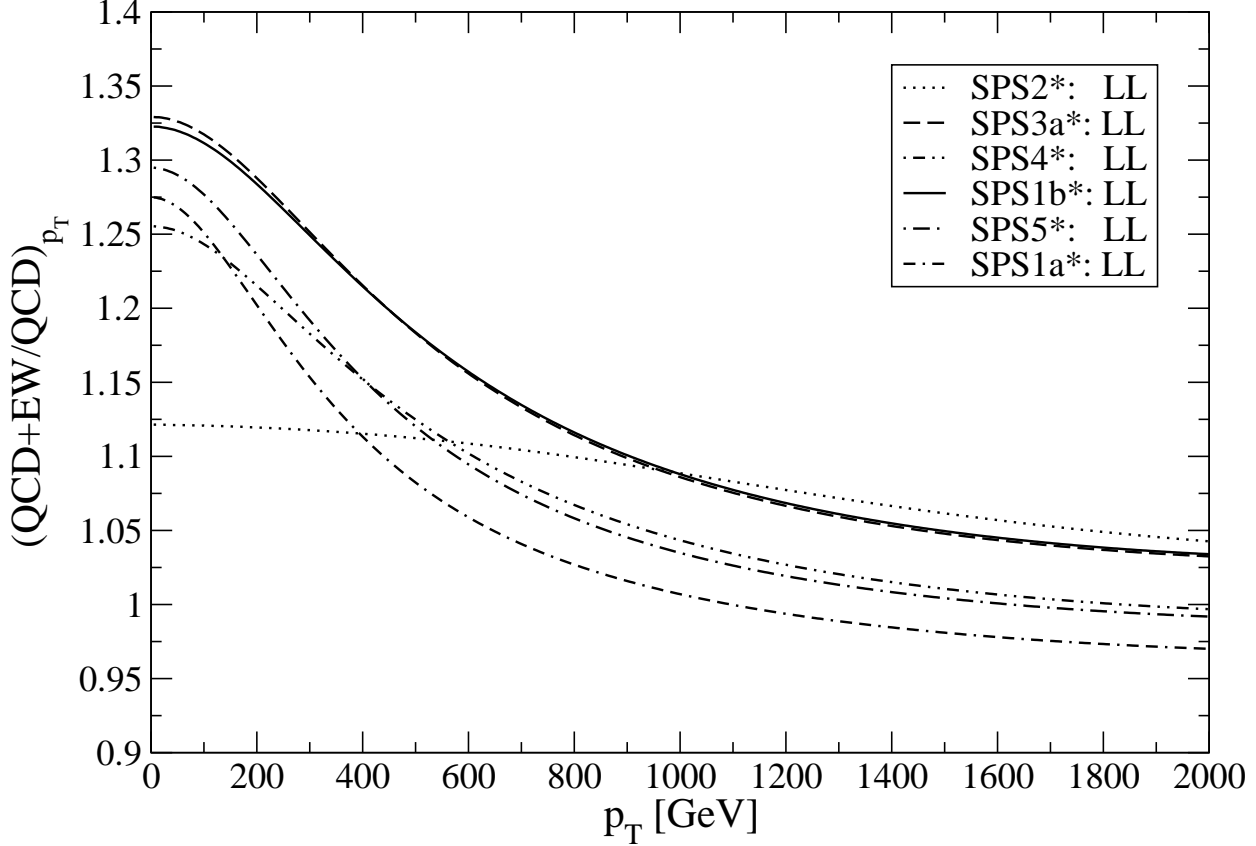


Figure 7: The ratio of QCD+EW to pure QCD predictions for the production of two $SU(2)$ doublet (anti-)squarks at the LHC as a function of the squark transverse momentum. We use the same mSUGRA scenarios as in Table 1.

preferred if p_T is sizable.

On the other hand, the denominators of the t -channel propagators can be written as

$$\hat{t} - M_{\tilde{V}}^2 = m_{\tilde{q}}^2 - \frac{\hat{s}}{2}(1 - \beta \cos \theta) - M_{\tilde{V}}^2, \quad (28)$$

where $M_{\tilde{V}}$ is the mass of the exchanged gaugino; the expression for u -channel propagators can be obtained by $\cos \theta \rightarrow -\cos \theta$. These propagators therefore prefer large $\beta|\cos \theta|$; however, t - and u -channel propagators prefer different signs of $\cos \theta$. We saw earlier that the dominant EW contributions are due to the interference between t - and u -channel diagrams (category 1 in Table 2). These cross sections are proportional to a single power of the threshold factor β . The steeply falling pdf's imply that these processes therefore prefer rather small values of

β even for small p_T . As a first approximation we can therefore ignore terms $\propto \beta \cos \theta$ in the propagators. The ratio of EW and QCD t - or u -channel propagators then becomes

$$\frac{\text{EW}}{\text{QCD}} = \frac{\hat{s}/2 - m_{\tilde{q}}^2 + M_{\tilde{g}}^2}{\hat{s}/2 - m_{\tilde{q}}^2 + M_{\tilde{W}}^2} \simeq \frac{2p_T^2 + m_{\tilde{q}}^2 + M_{\tilde{g}}^2}{2p_T^2 + m_{\tilde{q}}^2 + M_{\tilde{W}}^2}, \quad (29)$$

where $M_{\tilde{W}}$ is the mass of the relevant chargino or neutralino. Most of the mSUGRA scenarios of Table 1 and Fig. 7 have $m_{\tilde{q}}^2 \sim M_{\tilde{g}}^2 \gg M_{\tilde{W}}^2$. Eq.(29) shows that the interference term will then be enhanced by a factor ~ 2 at small p_T . However, this enhancement disappears for $m_{\tilde{q}}^2 \gg M_{\tilde{g}}^2$, as in SPS 2.

Eq.(29) shows that the propagator enhancement of the EW contributions also disappears once $2p_T^2 \gg m_{\tilde{q}}^2$. However, at large p_T the processes of category 1 may no longer be dominant even if we insist on having two $SU(2)$ doublet (anti-)squarks in the final state. We saw earlier that these processes require a helicity flip, i.e. their amplitudes are proportional to the mass of the exchanged gaugino. Dimensional arguments imply that the resulting product of two gaugino masses in these cross sections has to be compensated by an extra factor of p_T^{-2} for large p_T , relative to the processes without helicity flip. Table 2 shows that only category 2 processes can produce two doublet squarks without helicity flip. Here the interference between QCD and EW diagrams is destructive. If these processes dominate at large p_T , as implied by p_T power counting, EW contributions should therefore lead to a suppression of the cross section in this region of phase space. However, we also saw above that all category 2 processes require an anti-quark in the initial state. The relevant parton fluxes therefore fall much faster with increasing \hat{s} than for some of the category 1 processes. At large p_T one therefore has two competing suppression factors: category 1 processes, where EW contributions enhance the cross section, are suppressed by an extra p_T^{-2} , while category 2 processes are suppressed by more quickly falling pdf's. Eq.(27) shows that the latter suppression will be more relevant for larger squark masses. Indeed, at large p_T we observe the largest (or least negative) EW contributions for scenarios with heaviest squarks. However, even in scenario SPS1a, which has the smallest squark masses, EW contributions only suppress the cross section by $\sim 3\%$ at large p_T ; category 2 processes do contribute significantly here, but do not really dominate.

We saw in Table 1 that the EW contributions tend to become more important with increasing squark mass scale. This is further explored in Fig. 8, which shows the ratio of the total cross section for the production of $SU(2)$ doublet squarks with and without EW contributions as function of the average doublet squark mass. These curves have been generated by keeping the ratios of the dimensionful mSUGRA input parameters m_0 , $m_{1/2}$ and A_0 fixed, but varying the overall mass scale; this corresponds to the “benchmark slopes” of ref.[14]. We see that in a scenario with relatively large gaugino masses, as in SPS 1a (upper curve), the EW contribution can increase the cross section by more than 30% for $m_{\tilde{q}} = 2$ TeV. The cross section for much heavier squarks is too small for them to be detectable at the LHC. A scenario⁵ with $m_0 = -A_0 = 4.5m_{1/2}$ (lower curve) shows the same trend; however, as noted earlier, the total EW contribution is much smaller in this case, only reaching 13% for $m_{\tilde{q}} = 2$ TeV.

Note that the maximal relative size of the EW contribution in Fig. 8 exceeds that of the most favorable single process in Table 2. The results of this Figure can therefore not be

⁵This curve includes a scenario very similar to SPS 2; however, the corresponding slope defined in [14] does not permit small squark masses.

entirely due to the change of the relative weights of the various processes, as described in our discussion of Table 1. On top of that, the importance of the EW contributions to single processes increases with increasing squark masses. This can be understood from the behavior of the t - and u -channel propagators. Smaller squark masses allow larger values of β . The regions of phase space with large $|\cos\theta|$ will then favor the squared t - or u -channel propagators of pure QCD contributions over the product of one t - and one u -channel propagator of the interference terms. This implies that increasing $m_{\tilde{q}}$ will increase the relative importance of the interference terms relative to the squared t - and u -channel diagrams. This reduces the pure QCD contribution, where the interference is destructive due to the negative color factor, see e.g. Eq.(4), and enhances the importance of the EW contributions.

Comparison of the two curves in Fig. 8 reinforces the importance of the gaugino masses. So far we have considered sparticle spectra generated with mSUGRA boundary conditions. In particular, this implies that $SU(2)$ and $U(1)_Y$ gauginos are much lighter than gluinos. Since the dominant EW contributions (from category 1 in Table 2) are proportional to the product of the gluino mass with the mass of an electroweak gaugino, we expect that these contributions are sensitive to the assumed ratio of gaugino masses.

This is demonstrated in Fig. 9, where we vary the $SU(2)$ gaugino mass M_2 at the weak scale, keeping all other parameters fixed. We see that the electroweak contributions become maximal if $M_2 \simeq m_{\tilde{g}}$.⁶ This can be understood from the observation that this choice maximizes $M_2/|\hat{t} - M_2^2|$, see Eq.(28). In a scenario with $m_{\tilde{g}} \simeq m_{\tilde{q}}$ and large squark mass (solid curve), this can lead to EW contributions in excess of 50%. In scenario SPS 2 (dashed curve) the contributions remain somewhat smaller, partly because of the reduced squark mass, and partly because the lower gluino mass reduces the importance of the interference terms. Not surprisingly, taking $m_{\tilde{g}} \simeq m_{\tilde{q}}$ also maximizes the size of those pure QCD contributions that require a helicity flip.⁷ Finally, in scenario SPS 1a with its relatively light squarks (dotted curve) the EW contribution never goes much beyond 20%. We saw in Table 2 that in this case the processes of category 2 still contribute significantly. Here the EW contributions are negative. Since these processes do not require a helicity flip, the absolute size of the EW contributions decreases monotonically with increasing $|M_2|$. As a result, the dotted curve reaches its maximum for somewhat larger values of M_2 ; moreover, the maximum is less pronounced.

In Fig. 9 we show results as function of the weak scale soft breaking parameter M_2 , normalized to the squark mass. This parameter can be negative. If we keep the sign of the gluino mass parameter positive, the sign of the $t - u$ interference terms, which require a helicity flip, will change.⁸ We see that taking M_2 large and negative will lead to cross sections that are sig-

⁶The phenomenology of models with large $SU(2)$ gaugino mass parameter has recently been discussed in [23]; however, EW contributions to squark pair production were not considered in that paper.

⁷Maximizing the cross section with respect to M_2 and $m_{\tilde{g}}$ would prefer $m_{\tilde{g}}$ slightly below M_2 . The reason is that, as emphasized repeatedly, the main EW effect is due to interference between u - and t -channel diagrams. The corresponding mixed product of propagators has no strong preference for large $|\cos\theta|$. We saw above that, as a result, the denominator of the propagators are only moderately enhanced if the mass of the exchanged fermion is reduced. In contrast, the dominant QCD contributions come from squared t - and u -channel diagrams. Here the propagators do show stronger preference for sizable $|\cos\theta|$, and hence to a smaller mass of the exchanged fermion.

⁸One can write the amplitudes also entirely in terms of physical, positive masses. A negative M_2 would then need an extra factor i for each coupling of an $SU(2)$ gaugino, giving an extra $i^2 = -1$ for the $SU(2)$ amplitude relative to the QCD amplitude.

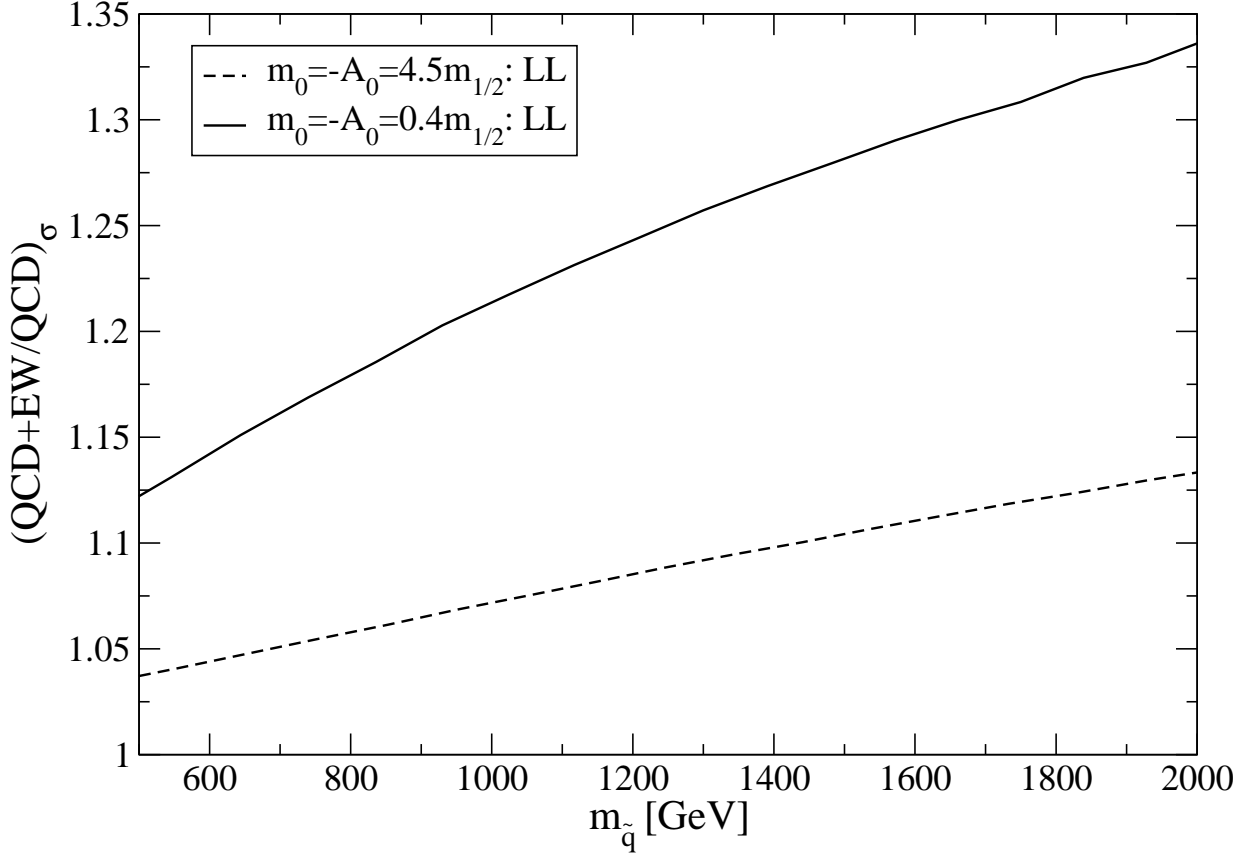


Figure 8: The ratio of QCD+EW to pure QCD predictions for the production of two $SU(2)$ doublet (anti-)squarks at the LHC as a function of the squark mass. The upper (lower) curve is for $m_0 = 0.4m_{1/2}$ ($m_0 = 4.5m_{1/2}$), with the overall scale of these soft breaking parameters being varied.

nificantly reduced from the pure QCD contribution. The relative size of the EW contributions is slightly smaller than that for positive M_2 . This is partly because we did not change the sign of the $U(1)_Y$ gaugino mass, keeping the corresponding contribution positive (but very small). Moreover, the cross sections for the (subdominant) category 2 processes remain essentially unchanged when the sign of M_2 is flipped; recall that category 3 processes do not contribute here. Altogether we see that the total cross section for the production of two $SU(2)$ (anti-)squarks can change by up to a factor 2.5 as M_2 is varied between $-m_{\tilde{q}}$ and $m_{\tilde{q}}$, if squarks are quite heavy and $m_{\tilde{g}} \simeq m_{\tilde{q}}$.

As discussed earlier, EW contributions will be much smaller if at least one (anti-)squark in

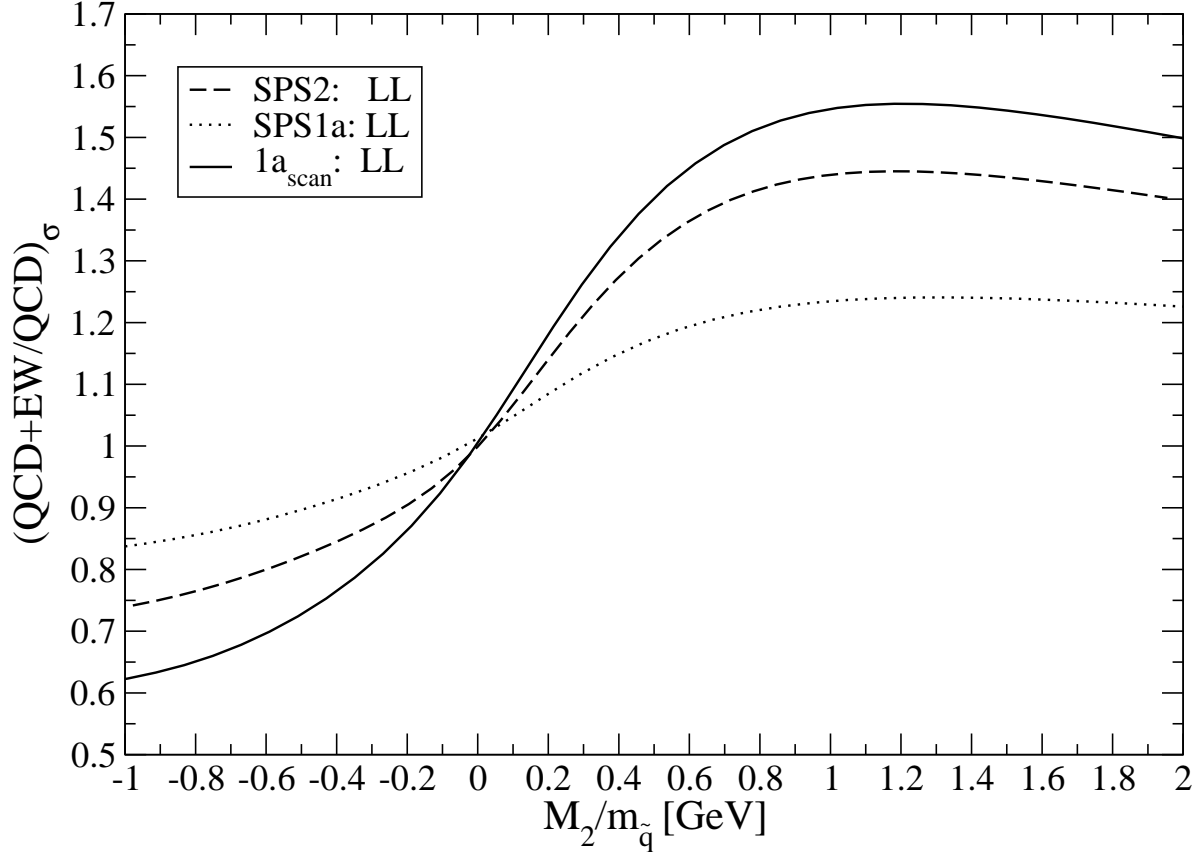


Figure 9: The ratio of QCD+EW to pure QCD predictions for the production of two $SU(2)$ doublet (anti-)squarks at the LHC as a function of the ratio of the $SU(2)$ gaugino mass parameter M_2 and the squark mass. The solid and dotted curves are both based on scenario SPS 1a of Table 1, but for the solid curve all soft breaking masses have been scaled up to achieve a squark mass of 2 TeV. The dashed curve is for scenario SPS 2. In all cases M_2 has been varied directly at the weak scale using SPheno [22], leaving all other weak-scale soft breaking parameters unchanged.

the final state is an $SU(2)$ singlet. However, it might well be possible to experimentally separate these different classes of final states. At least for $m_{\tilde{g}} \gtrsim m_{\tilde{q}} > |M_2|, |M_1|$ the production of two doublet squarks leads to significantly different final states than that of singlet squarks. The former prefer to decay into charginos and neutralinos dominated by $SU(2)$ gaugino components [24]; in mSUGRA, this typically means $\tilde{\chi}_2^0$ and $\tilde{\chi}_1^\pm$. This leads to longer decay chains than for $SU(2)$ singlet squarks, which prefer to decay into the neutralino with the largest bino component

[24], in mSUGRA usually $\tilde{\chi}_1^0$. The contribution of doublet squarks can therefore be enhanced experimentally by requiring the presence of energetic, isolated charged leptons (electrons or muons), in addition to ≥ 2 jets and missing transverse momentum [25]. If $m_{\tilde{g}} < m_{\tilde{q}}$ this distinction becomes more difficult, since then most squarks decay into a gluino and a quark; however, the branching ratio for $SU(2)$ doublet squark decays into charginos and neutralinos remains sizable even in this case. Similarly, in models with explicit violation of R -parity, $SU(2)$ doublet squarks may have very different decay channels than singlets [26].

4 Summary and Conclusions

In this paper we analyzed electroweak (EW) contributions to the production of two squarks or anti-squarks at the LHC. We provided explicit expressions for the squared matrix elements for all processes with (anti-)quarks in the initial state, allowing for different squark masses in the final state. Not surprisingly, corrections due to $SU(2)$ interactions are more important than those from $U(1)_Y$ interactions. In both cases the dominant effect is from the interference of electroweak and QCD interactions. The sign of the interference between EW t - and QCD u -channel diagrams (or vice versa) is positive (negative) for equal (opposite) signs of the electroweak and QCD gaugino mass parameters. Interference between EW t - and QCD s -channel diagrams (or vice versa) is usually negative, and independent of the sign of the gaugino mass parameters.

The physical significance of our results is threefold:

- The EW contributions can change the total cross section significantly. Focusing on the production of two $SU(2)$ doublet (L -type) squarks, we found the contributions with interference between t - and u -channel diagrams to be dominant. For squark masses near the discovery reach of the LHC, EW effects can reduce or enhance the total cross section by more than a factor 1.5, if the absolute value of the $SU(2)$ gaugino soft breaking mass is near $m_{\tilde{q}}$; even in scenarios with gaugino mass unification the EW contribution can still change the cross section for the production of two $SU(2)$ doublet squarks by more than a factor 1.3. Recall that $SU(2)$ doublet squarks often lead to different final states than singlet squarks do, allowing to distinguish these modes experimentally.
- The EW contributions might give a new, independent handle on the gaugino mass parameters. In particular, we just saw that they are sensitive to relative *signs* between gaugino mass parameters, which might be difficult to determine using kinematical distributions only. For example, in anomaly-mediated supersymmetry breaking [27] the products of electroweak and QCD gaugino masses are negative. In order to realize this potential, both the experimental and the theoretical uncertainties should be reduced to the 10% level. This is certainly challenging, but should eventually be possible if squarks are not too heavy.
- The EW contributions allow production of two squarks without color connection between the squarks. In contrast, at least in leading order QCD diagrams for squark production, there is color flow between the two squarks. The absence of such a flow could in principle give rise to a rapidity gap, i.e. a rapidity region into which no QCD radiation is emitted;

such radiation would then only occur in the region between the squark and the quark from which it was produced (and from which it inherited its color). This is completely analogous to the gap predicted for ordinary (non-supersymmetric) two-jet events produced at hadron colliders via electroweak interactions [28]. We are currently investigating if such supersymmetric rapidity gap events might be detectable at the LHC.

Acknowledgments

This work was partially supported by the Bundesministerium für Bildung und Forschung under contract no. 05HT6PDA. SB thanks the Universitätsgesellschaft Bonn – Freunde, Förderer, Alumni e.V. for financial support.

A Couplings

In this Appendix we give explicit expressions for all the couplings appearing in Sec. 2, using the notation of [18]. We only list couplings of squarks. The corresponding couplings of anti-squarks can be obtained using relations (6) and (10).

A.1 Neutralino and Gluino Couplings

Since gluino and neutralino exchange always occur together, we labeled them with the subscript l , with $l \in \{1, 2, 3, 4\}$ denoting the l -th neutralino mass eigenstate and $l = 5$ denoting the gluino. Here we need the left- and right-handed quark-squark-gaugino couplings, generically denoted by a and b , respectively. The relevant **neutralino couplings** are:

$$\begin{aligned}
a_{\tilde{\chi}_l^0}(\tilde{d}_{i\alpha}) &= -\delta_{1\alpha}\sqrt{2}g\left(\frac{1}{2}N_{l2}^* - \frac{1}{6}\tan\theta_W N_{l1}^*\right), \\
b_{\tilde{\chi}_l^0}(\tilde{d}_{i\alpha}) &= \delta_{2\alpha}\frac{\sqrt{2}}{3}g\tan\theta_W N_{l1}, \\
a_{\tilde{\chi}_l^0}(\tilde{u}_{i\alpha}) &= \delta_{1\alpha}\sqrt{2}g\left(\frac{1}{2}N_{l2}^* + \frac{1}{6}\tan\theta_W N_{l1}^*\right), \\
b_{\tilde{\chi}_l^0}(\tilde{u}_{i\alpha}) &= -\delta_{2\alpha}\frac{2\sqrt{2}}{3}g\tan\theta_W N_{l1}.
\end{aligned} \tag{30}$$

Here $\alpha = 1$ (2) stands for an L – (R)-type squark, and N_{l1} and N_{l2} stand for the $U(1)_Y$ (bino) and $SU(2)$ (neutral wino) components of $\tilde{\chi}_l^0$, respectively. Recall that we ignore quark mass effects, and hence also Yukawa contributions to the neutralino couplings. Finally, g is the $SU(2)$ gauge coupling, and θ_W is the weak mixing angle.

The corresponding **gluino couplings** are:

$$\begin{aligned}
a_{\tilde{g}}(\tilde{d}_{i\alpha}) &= -\delta_{1\alpha}g_s\sqrt{2}, \\
b_{\tilde{g}}(\tilde{d}_{i\alpha}) &= \delta_{2\alpha}g_s\sqrt{2}, \\
a_{\tilde{g}}(\tilde{u}_{i\alpha}) &= -\delta_{1\alpha}g_s\sqrt{2}, \\
b_{\tilde{g}}(\tilde{u}_{i\alpha}) &= \delta_{2\alpha}g_s\sqrt{2},
\end{aligned} \tag{31}$$

where g_s is the $SU(3)$ gauge coupling.

A.2 Chargino Couplings

For a given process, charginos cannot be exchanged in diagrams of the same topology as neutralinos and gluinos. Here the subscript l labeling the exchanged particle therefore only runs from 1 to 2, corresponding to the two chargino mass eigenstates in the MSSM. Their relevant couplings are:

$$\begin{aligned}
a_{\chi_l^+}(\tilde{d}_{i\alpha}) &= -gU_{l1}\delta_{1\alpha}, \\
b_{\chi_l^+}(\tilde{d}_{i\alpha}) &= 0, \\
a_{\chi_l^+}(\tilde{u}_{i\alpha}) &= -gV_{l1}\delta_{1\alpha}, \\
b_{\chi_l^+}(\tilde{u}_{i\alpha}) &= 0.
\end{aligned} \tag{32}$$

The vanishing of the right-handed, b -type couplings is again due to our neglect of Yukawa couplings.

A.3 Gauge Boson Couplings

Here (s -channel) diagrams with photon, Z boson and gluon exchange always occur together. We therefore labeled these particles with subscript l , $l = 1, 2, 3$ standing for the γ , Z boson and gluon, respectively. e and f represent the left- and right-handed gauge boson-quark-anti-quark couplings,

$$\begin{aligned}
e_\gamma(d_i, \bar{d}_i) &= f_\gamma(d_i, \bar{d}_i) = \frac{1}{3}g \sin \theta_W, \\
e_\gamma(u_i, \bar{u}_i) &= f_\gamma(u_i, \bar{u}_i) = -\frac{2}{3}g \sin \theta_W, \\
e_Z(d_i, \bar{d}_i) &= \frac{g}{\cos \theta_W} \frac{1}{2} \left(1 - \frac{2}{3} \sin^2 \theta_W \right), \\
f_Z(d_i, \bar{d}_i) &= -\frac{g}{\cos \theta_W} \frac{1}{3} \sin^2 \theta_W, \\
e_Z(u_i, \bar{u}_i) &= -\frac{g}{\cos \theta_W} \frac{1}{2} \left(1 - \frac{4}{3} \sin^2 \theta_W \right), \\
f_Z(u_i, \bar{u}_i) &= \frac{g}{\cos \theta_W} \frac{2}{3} \sin^2 \theta_W, \\
e_g(d_i, \bar{d}_i) &= f_g(d_i, \bar{d}_i) = e_g(u_i, \bar{u}_i) = f_g(u_i, \bar{u}_i) = -g_s.
\end{aligned} \tag{33}$$

Their couplings to a squark and an anti-squark, generically denoted by c , are:

$$\begin{aligned}
c_\gamma(\tilde{d}_{i\alpha}, \bar{\tilde{d}}_{i\alpha}) &= \frac{1}{3}g \sin \theta_W, \\
c_\gamma(\tilde{u}_{i\alpha}, \bar{\tilde{u}}_{i\alpha}) &= -\frac{2}{3}g \sin \theta_W, \\
c_Z(\tilde{d}_{i\alpha}, \bar{\tilde{d}}_{i\alpha}) &= \frac{g}{\cos \theta_W} \frac{1}{2} \left(\delta_{1\alpha} - \frac{2}{3} \sin^2 \theta_W \right), \\
c_Z(\tilde{u}_{i\alpha}, \bar{\tilde{u}}_{i\alpha}) &= \frac{g}{\cos \theta_W} \frac{1}{2} \left(-\delta_{1\alpha} + \frac{4}{3} \sin^2 \theta_W \right), \\
c_g(\tilde{d}_{i\alpha}, \bar{\tilde{d}}_{i\alpha}) &= c_g(\tilde{u}_{i\alpha}, \bar{\tilde{u}}_{i\alpha}) = -g_s.
\end{aligned} \tag{34}$$

Note that in the absence of $L - R$ mixing, the couplings listed in Eq.(34) are nonzero only if both the squark and the anti-squark are $SU(2)$ doublets ($\alpha = 1$), or both are singlets ($\alpha = 2$).

Finally, in some cases there are s -channel diagrams in which a W -boson is exchanged. Its couplings to the initial state are given by

$$\begin{aligned} e_W(d_i, \bar{u}_i) &= e_W(u_i, \bar{d}_i) = -\frac{g}{\sqrt{2}}, \\ f_W(d_i, \bar{u}_i) &= f_W(u_i, \bar{d}_i) = 0, \end{aligned} \quad (35)$$

and the relevant final state couplings are

$$c_W(\tilde{d}_{i\alpha}, \bar{\tilde{u}}_{i\alpha}) = c_W(\tilde{u}_{i\alpha}, \bar{\tilde{d}}_{i\alpha}) = -\frac{g}{\sqrt{2}}\delta_{1\alpha}. \quad (36)$$

References

- [1] For introductions to supersymmetry, see e.g. M. Drees, R.M. Godbole and P. Roy, *Theory and Phenomenology of Sparticles*, World Scientific Publishing Company (2004); H. Baer and X. Tata, *Weak Scale Supersymmetry: From Superfields to Scattering Events*, Cambridge, UK: Univ. Pr. (2006).
- [2] E. Witten, Nucl. Phys. **B188**, 513 (1981); N. Sakai, Z. Phys. **C11**, 153 (1981); S. Dimopoulos and H. Georgi, Nucl. Phys. **B193**, 150 (1981); R.K. Kaul and P. Majumdar, Nucl. Phys. **B199**, 36 (1982).
- [3] J. Ellis, S. Kelley and D.V. Nanopoulos, Phys. Lett. B260 (1991) 131; U. Amaldi, W. de Boer and H. Fürstenau, Phys. Lett. B260 (1991) 447; P. Langacker and M. Luo, Phys. Rev.D 44 (1991) 817; C. Giunti, C.W. Kim and U.W. Lee, Mod. Phys. Lett. A6 (1991) 1745.
- [4] For a review, see G. Jungman, M. Kamionkowski and K. Griest, Phys. Rep. **267** (1996) 195, hep-ph/9506380.
- [5] WMAP Collab., D.N. Spergel et al., Astrophys. J. Suppl. **148**, 175 (2003), astro-ph/0302209; WMAP Collab., D.N. Spergel et al., Astrophys. J. Suppl. **170**, 377 (2007), astro-ph/0603449.
- [6] J.A. Grifols and A. Mendez, Phys. Rev. **D26**, 1809 (1982); J.R. Ellis, J.S. Hagelin and D.V. Nanopoulos, Phys. Lett. **B116**, 283 (1982); R. Barbieri and L. Maiani, Phys. Lett. **B117**, 203 (1982); T.C. Yuan, R. Arnowitt, A. H. Chamseddine and P. Nath, Z. Phys. **C26**, 407 (1984); S.P. Martin and J.D. Wells, Phys. Rev. D64 (2001) 035003, hep-ph/0103067.
- [7] Muon $g - 2$ Collab., G.W. Bennett et al., Phys. Rev. Lett. **89**, 101804 (2002), Erratum-ibid. **89**, 129903 (2002), hep-ex/0208001, and Phys. Rev. Lett. **92**, 161802 (2004), hep-ex/0401008.

- [8] M. Davier, S. Eidelman, A. Höcker and Z. Zhang, Eur. Phys. J. **C31**, 503 (2003), hep-ph/0308213; K. Hagiwara, A.D. Martin, D. Nomura and T. Teubner, Phys. Rev. **D69**, 093003 (2004), hep-ph/0312250, and Phys. Lett. **B649**, 173 (2007), hep-ph/0611102; J.F. de Troconiz and F.J. Yndurain, Phys. Rev. **D71**, 073008 (2005), hep-ph/0402285; M. Passera, J. Phys. **G31**, R75 (2005), hep-ph/0411168; F. Jegerlehner, hep-ph/0703125.
- [9] J.R. Ellis, S. Heinemeyer, K.A. Olive, A.M. Weber and G. Weiglein, arXiv:0706.0652 [hep-ph].
- [10] ATLAS collab., *Detector and physics performance technical design report*, Vol. 2, Ch. 20, CERN-LHCC-99-15; CMS Collab., S. Abdullin et al., J. Phys. **G28**, 469 (2002), hep-ph/9806366.
- [11] P.R. Harrison and C.H. Llewellyn Smith, Nucl. Phys. **B213**, 223 (1983); Erratum ibid. **B223**, 542 (1983); S. Dawson, E. Eichten and C. Quigg, Phys. Rev. **D31**, 1581 (1985); H. Baer and X. Tata, Phys. Lett. **B160**, 159 (1985).
- [12] W. Beenakker, R. Hopker, M. Spira and P.M. Zerwas, Phys. Rev. Lett. **74**, 2905 (1995), hep-ph/9412272, and Nucl. Phys. **B492**, 51 (1997), hep-ph/9610490.
- [13] A.H. Chamseddine, R. Arnowitt and P. Nath, Phys. Rev. Lett. **49** (1982) 970; R. Barbieri, S. Ferrara and C.A. Savoy, Phys. Lett. **B119** (1982) 343; L. Hall, J. Lykken and S. Weinberg, Phys. Rev. **D27** (1983) 2359.
- [14] B.C. Allanach et al., presented at *APS / DPF / DPB Summer Study on the Future of Particle Physics (Snowmass 2001)*, Snowmass, Colorado, 30 Jun - 21 Jul 2001, hep-ph/0202233.
- [15] K. Choi and H.P. Nilles, JHEP **0704**, 006 (2007), hep-ph/0702146.
- [16] G. Bozzi, B. Fuks, B. Herrmann and M. Klasen, arXiv:0704.1826 [hep-ph].
- [17] A.T. Alan, K. Cankocak and D.A. Demir, Phys. Rev. **D75**, 095002 (2007), hep-ph/0702289.
- [18] J.F. Gunion and H.E. Haber, Nucl. Phys. **B272**, 1 (1986), Erratum-ibid. **B402**, 567 (1993).
- [19] Particle Data Group, W.-M. Yao et al., J. Phys. **G33**, 1 (2006).
- [20] CTEQ Collab., H.L. Lai et al., Eur. Phys. J. **C12**, 375 (2000), hep-ph/9903282.
- [21] B.C. Allanach, Comput. Phys. Commun. **143**, 305 (2002), hep-ph/0104145.
- [22] W. Porod, Comput. Phys. Commun. **153**, 275 (2003), hep-ph/0301101.
- [23] H. Baer, A. Mustafayev, H. Summy and Xerxes Tata arXiv:0708.4003.
- [24] H. Baer, V.D. Barger, D. Karatas and X. Tata, Phys. Rev. **D36**, 96 (1987).

- [25] M.M. Nojiri and M. Takeuchi, Phys. Rev. **D76**, 015009 (2007), hep-ph/0701190.
- [26] B.C. Allanach, M.A. Bernhardt, H.K. Dreiner, C.H. Kom and P. Richardson, Phys. Rev. **D75**, 035002 (2007), hep-ph/0609263.
- [27] G.F. Giudice, M.A. Luty, H. Murayama and R. Rattazzi, JHEP **9812**, 027 (1998), hep-ph/9810442; L. Randall and R. Sundrum, Nucl. Phys. **B557**, 79 (1999), hep-th/9810155.
- [28] H. Chehime, M.B. Gay Ducati, A. Duff, F. Halzen, A.A. Natale, T. Stelzer and D. Zeppenfeld, Phys. Lett. **B286**, 397 (1992).